Demographic history explains mitochondrial genome capture and mitonuclear discordance among South American collared *Tropidurus* lizards

Matheus M. A. Salles[1*], André L. G. Carvalho[2], Adam D. Leaché[2], Nicolas Martinez[3], Frederick Bauer[3], Martha Motte[3], Viviana Espínola[3], Miguel T. Rodrigues[4], Carla Piantoni[5], Marcio R. Pie[1], André Olivotto[1], Guarino R. Colli[6], Erik L. Choueri[7], Fernanda P. Werneck[7], Fabricius M. C. B. Domingos[1]

[1] Programa de Pós-graduação em Zoologia, Universidade Federal do Paraná, Curitiba/PR, Brasil

[2] Department of Biology & Burke Museum of Natural History and Culture, University of Washington, Seattle/WA, USA

[3] Museo Nacional de Historia Natural del Paraguay, Asuncion, Paraguay

[4] Instituto de Biociências da Universidade de São Paulo, São Paulo/SP, Brasil

[5] School of Life Sciences, University of Hawaii at Manoa, Honolulu/HI, USA

[6] Departamento de Zoologia, Universidade de Brasília, Brasília/DF, Brasil

[7] Programa de Coleções Científicas Biológicas, Coordenação de Biodiversidade, Instituto Nacional de Pesquisas da Amazônia, Manaus/AM, Brasil

[*]*Author for Correspondence*: Matheus Salles, Programa de Pós-Graduação em Zoologia, Universidade Federal do Paraná (Departamento de Zoologia, Setor de Ciências Biológicas, Centro Politécnico, Avenida Cel. Francisco H Santos, Jardim das Américas, 81531-980, Curitiba/PR, Brasil), matheus.salles@ufpr.br.

Abstract

Mitonuclear discordance—evolutionary discrepancies between mitochondrial and nuclear DNA phylogenies—can arise from various factors, including introgression, incomplete lineage sorting, recent or ancient demographic fluctuations, sex-biased dispersal asymmetries, among others. Understanding this phenomenon is crucial for accurately reconstructing evolutionary histories, as failing to account for discordance can lead to misinterpretations of species boundaries, phylogenetic relationships, and historical biogeographic patterns. In this study, we investigate the evolutionary drivers of mitonuclear discordance in the *Tropidurus spinulosus* species group, which contains nine species of lizards inhabiting open tropical and subtropical environments in South America. Using a combination of population genetic and phylogenomic approaches, applied to mitochondrial and nuclear data, we identified different instances of gene flow that occurred in ancestral lineages of extant species. Our results point to a complex evolutionary history marked by prolonged isolation between species, demographic fluctuations, and potential episodes of secondary contact with genetic admixture. These conditions likely facilitated mitochondrial genome capture while diluting signals of nuclear introgression. Furthermore, we found no strong evidence supporting incomplete lineage sorting or natural selection as primary drivers of the observed mitonuclear discordance. Therefore, the unveiled patterns are most consistent with neutral demographic processes, coupled with ancient mitochondrial introgression, as the main factors underlying the mismatch between nuclear and mitochondrial phylogenies in this system. Future research could further explore the role of other demographic processes, such as asymmetric sex-biased dispersal, in shaping these complex evolutionary patterns.

Key words: Mitogenome; Molecular Evolution; Phylogenomics; Squamata; Tropiduridae.

Significance

Mitochondrial and nuclear genomes evolve independently, through distinct processes, often leading to conflicting genetic patterns—a phenomenon known as mitonuclear discordance. While widely documented, the underlying causes of such discordant patterns are not always clear. In this study, we investigated the drivers of mitonuclear discordance using a lizard group (the *Tropidurus spinulosus* species group) as a model system. Our findings suggest that changes in population size and historical isolation, possibly followed by secondary contact, were key drivers of ancient introgression among species, especially affecting the mitochondrial genome. These results provide valuable insights into how natural population dynamics shape the evolutionary processes behind mitonuclear discordance.

Introduction

Mitochondrial and nuclear genomes evolve independently, through distinct processes, often leading to conflicting genetic patterns—a phenomenon known as mitonuclear discordance. Cases of mitonuclear discordance are increasingly reported across a wide range of animal species. Recent examples can be found among mammals (Good et al. 2015; Phuong et al. 2016; Seixas et al. 2018; Fedorov et al. 2022), birds (Andersen et al. 2021; DeRaad et al. 2023), reptiles (Firneno et al. 2021), amphibians (Zieliński et al. 2013; Dufresnes et al. 2020; Rancilhac et al. 2021), and insects (Hinojosa et al. 2019; Dong et al., 2023). Generally, conflicting patterns between nuDNA and mtDNA arise from processes such as introgression, demographic fluctuations, sex-biased dispersal asymmetries, incomplete lineage sorting (ILS), human introductions, or *Wolbachia* infection in insects (see reviews by Toews and Brelsford 2012; Bonnet et al. 2017; Deprés 2019). Determining whether mitonuclear discordance is driven by any of these factors requires a clear understanding of the genealogies among

73 different loci, the demographic history of populations, and their historical
74 introgression/migration patterns and rates. Notably, these complexities often present
75 significant empirical challenges in resolving the underlying causes of discordance.

76 Most cases of discordance are attributed to mtDNA introgression (Toews and Brelsford
77 2012) and are generally associated with processes such as gene flow across hybrid zones
78 (Zieliński et al. 2013; Good et al. 2015; Dufresnes et al. 2020; Mao and Rossiter 2020) and
79 mitochondrial capture (Andersen et al. 2021). The latter refers specifically to a form of
80 complete introgression, where the mitochondrial genome of one species is entirely replaced
81 by another's (Zieliński et al. 2013). Mitochondrial capture can occur at various stages of the
82 speciation process and between distantly related species (Rancilhac et al. 2021). Additionally,
83 mitochondrial introgression can take place with minimal or not accompanying nuDNA
84 introgression (Zieliński et al. 2013; Good et al. 2015; Andersen et al. 2021; Rancilhac et al.
85 2021; Fedorov et al. 2022), making it challenging to detect introgressed nuclear and
86 mitochondrial markers simultaneously (Bonnet et al. 2017; Seixas et al. 2018). Therefore, ILS
87 is another phenomenon that cannot be overlooked in discussion of mitonuclear discordance,
88 given the challenges in distinguishing it from introgression (Andersen et al. 2021; DeRaad et
89 al. 2023). While some studies have identified ILS as a primary driver of mitonuclear
90 discordance, these remain relatively rare (e.g., Firneno et al. 2021).

91 Demographic factors, such as fluctuation in population sizes, particularly at the
92 periphery of a species' geographic range, can also contribute to mitonuclear discordance
93 (Phuong et al. 2016; Dufresnes et al. 2020; Fedorov et al. 2022). In this scenario, neutral
94 processes such as genetic drift can help in the fixation of mtDNA haplotypes at range edges of
95 expanding populations (Bonnet et al. 2017). Even in situations where introgression involves
96 both mtDNA and nuclear loci, mtDNA is expected to reach fixation faster, since it has a smaller

97 effective population size and is non-recombining (Moore 1995). Following demographic
98 expansions and secondary contact, nuclear genomes can fully recombine, thereby diluting
99 historical introgression signals, whereas divergent, non-recombining mitochondrial
100 haplotypes may persist.

101 Finally, selection can also play a role in generating mitonuclear discordance (Toews and
102 Brelsford 2012). If a beneficial mitochondrial mutation arises but is initially incompatible with
103 the nuclear genetic background of a population, selection may favor nuclear variants that
104 restore mitonuclear compatibility. This compensatory selection could lead to a scenario where
105 the advantageous mitochondrial mutation spreads widely, while the nuclear DNA follows a
106 different evolutionary trajectory. Empirical evidence robustly demonstrates that natural
107 selection can drive mtDNA introgression between populations through hybridization, even in
108 the absence of corresponding nuDNA introgression, provided there is even a minor selective
109 advantage (Excoffier et al. 2009; Zieliński et al. 2013; Good et al. 2015; Phuong et al. 2016). As
110 a result, the mitochondrial genome with the highest fitness may introgress into another
111 species, regardless of whether it originates from the resident or the invading population.

112 Here, we investigate the drivers of mitonuclear discordance in a biological system with
113 known occurrences of this phenomenon, the lizard family Tropiduridae (e.g., *Microlophus*:
114 Benavides et al. 2007; 2009; *Tropidurus*: Carvalho et al. 2016). Specifically, we explored the
115 evolutionary history of nine lineages within the *T. spinulosus* group using a multi-locus
116 genomic approach. This diverse group of lizards is distributed across open-vegetation tropical
117 and subtropical environments in South America and predominantly inhabit rocky and arboreal
118 habitats (Frost et al. 1998; Carvalho 2013, 2016; Carvalho et al. 2013). Although the taxonomy
119 of the *Tropidurus spinulosus* group has been relatively stable, new species continue to be
120 described (e.g., Carvalho 2016). Additionally, our research includes all taxa presently admitted

121 for the group plus one undescribed species, which is currently undergoing formal description
122 (Carvalho et al. in prep) and is referred to as *Tropidurus sp. nov.* in this study.

123 We integrated mitochondrial genomes, nuclear ultraconserved elements (UCEs), and
124 single nucleotide polymorphisms (SNPs) derived from UCEs to assess whether the
125 mitochondrial genealogy corresponded to reciprocally monophyletic nuclear lineages. To
126 determine the potential sources of the mitonuclear discordance, we examine the relative
127 contributions of neutral and selective processes. Specifically, we first compared mtDNA and
128 nuclear phylogenies to identify conflicts and potential introgression patterns, using methods
129 that either account for ILS or do not. In a scenario where these approaches yield largely
130 congruent results, this would suggest that ILS may not play a major role in the observed
131 mitonuclear discordance. Second, we evaluated whether mtDNA introgression was
132 accompanied by detectable levels of nuDNA introgression, as most cases of discordance are
133 attributed to processes such as gene flow across hybrid zones. We also assessed signals of
134 positive selection on mtDNA to evaluate potential adaptive processes in shaping mitonuclear
135 discordance. Finally, as demographic processes can contribute to emerging phylogenetic
136 discordant patterns as well, we examined historical changes in population size to assess their
137 role in shaping the observed discordance, as this would align with expectations under a non-
138 adaptive scenario.

139

140 **Results**

141 *UCE and mtDNA phylogenomic datasets*

142 After processing our data using the Phyluce pipeline (Faircloth 2016), we obtained a
143 final dataset including 820 UCE loci for 43 individuals of nine lineages of the *Tropidurus*
144 *spinulosus* species group. Our complete matrix comprised alignments with 725,505 bp after

145 internal-trimming. Matrices with 75% and 95% of completeness were also generated, which,
146 after internal-trimming, generated alignments with 2,269 and 1,613 loci, 1.98M and 1.40M
147 bp, respectively. Nuclear phylogenetic analyses using both a partitioned approach in the IQ-
148 TREE software (Minh et al. 2020), based on complete and incomplete matrices
149 (Supplementary Figures S1-S3), and a species tree approach based on BPP (Figure 1; Flouri et
150 al. 2018), indicated that our samples can be grouped into three main clades: (*T. sp. nov. + T.*
151 *xanthochilus), (T. lagunablanca + T. tarara), (T. guarani + T. spinulosus + T. teyumirim)*, in
152 addition to *T. callathelys and T. melanopleurus* as external lineages to the clade comprising
153 the remaining species. The trees inferred using ASTRAL (Zhang et al. 2018), which account for
154 ILS, produced similar patterns (Supplementary Figures S4-S6). Compared to the UCE dataset,
155 the mtDNA dataset (alignment with 40 samples, 15 genes, and 13,578 bp) produced markedly
156 different results regarding topology, indicating a clear case of mitonuclear discordance (Figure
157 1; Supplementary Figure S7-S8). Notably different from the nuclear trees, our mitochondrial
158 genealogy shows that while most *T. xanthochilus* samples were grouped as sister to the clade
159 containing *T. spinulosus* and *T. guarani*, two *T. xanthochilus* samples, the *T. sp. nov.* and the *T.*
160 *teyumirim* samples, were all recovered within the *T. tarara* + *T. lagunablanca* clade. Besides,
161 despite *T. xanthochilus* and *T. sp. nov.* forming a clade based on nuclear data, they do not
162 appear closely related in the mitochondrial dataset. Similarly, most groups observed in these
163 two phylogenetic trees are reflected in the haplotype network inferred for the *T. spinulosus*
164 group, showing the same pattern of discordance compared to the nuclear data
165 (Supplementary Figure S9).
166

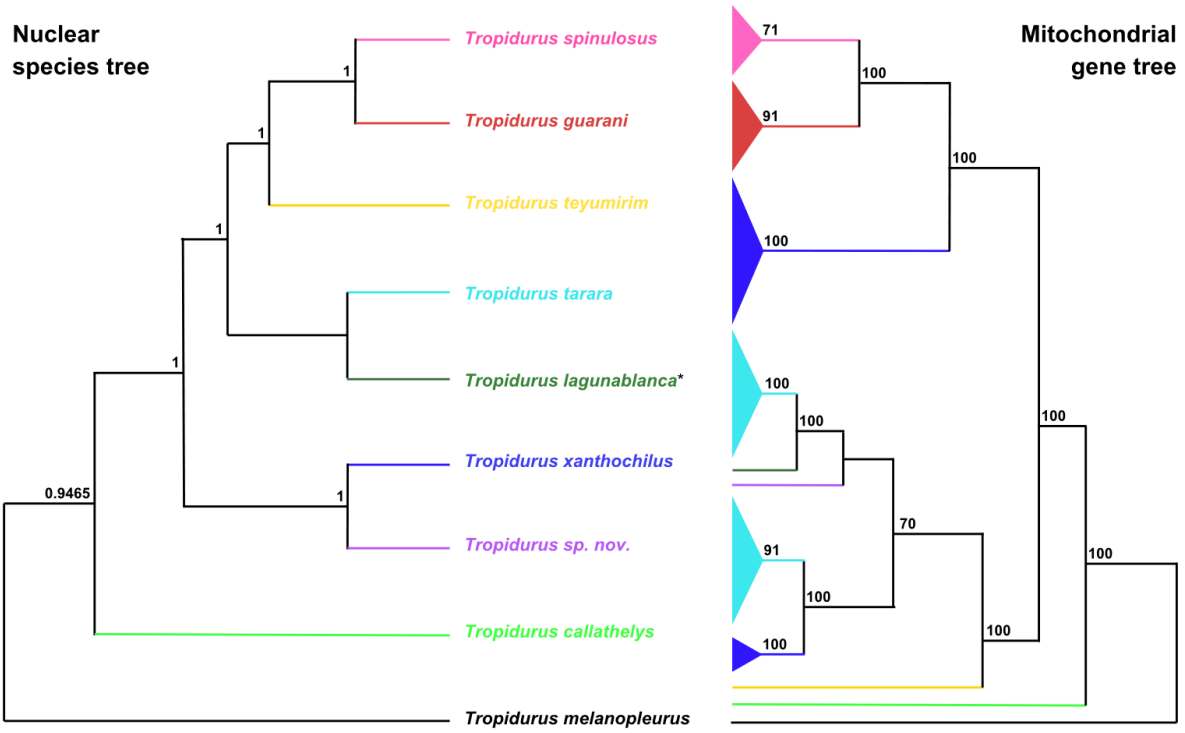

Fig. 1. Comparison between the nuclear species tree and the mitochondrial gene tree for the group *Tropidurus spinulosus*. The left panel shows the species tree inferred from multilocus nuclear data using BPP, with branch support values indicated next to nodes (posterior probabilities). The right panel displays the mitochondrial gene tree inferred through IQ-TREE, with branch support shown as bootstrap values (in this case, we only show values above 70). Colored clades correspond to the same taxa in both trees. Collapsed branches in the mitochondrial tree represent intraspecific variation (for the fully detailed tree, see the Supplementary Material). *All nuclear gene trees recovered *T. lagunablanca* nested within *T. tarara* samples, indicating that these lineages likely represent a single evolutionary unit. Accordingly, the *T. lagunablanca* sample was assigned to *T. tarara* in the BPP analysis, so that they represent a single branch in the estimated species tree. However, for a clearer comparison with the mitochondrial genealogy, in this figure we present the two lineages as separate branches within the same clade.

Divergence dating with nuclear data indicates that the initial split within the *Tropidurus spinulosus* group occurred between 20 and 15 million years ago (Ma), separating *T. melanopleurus* from the other lineages. The split involving *T. callathelys* occurred approximately 10 Ma ago, and most subsequent divergence events among the remaining species of the group took place between 7.5 and 2.5 Ma (Figure 2; Supplementary Figure S10). In most cases, the divergence times estimated using RelTime (Tamura et al. 2018) fall within the same 95% highest posterior density (HPD) intervals provided by MCMCTree (dos Reis and Yang 2019), but some differences can be noticed (Supplementary Figure S10-11).

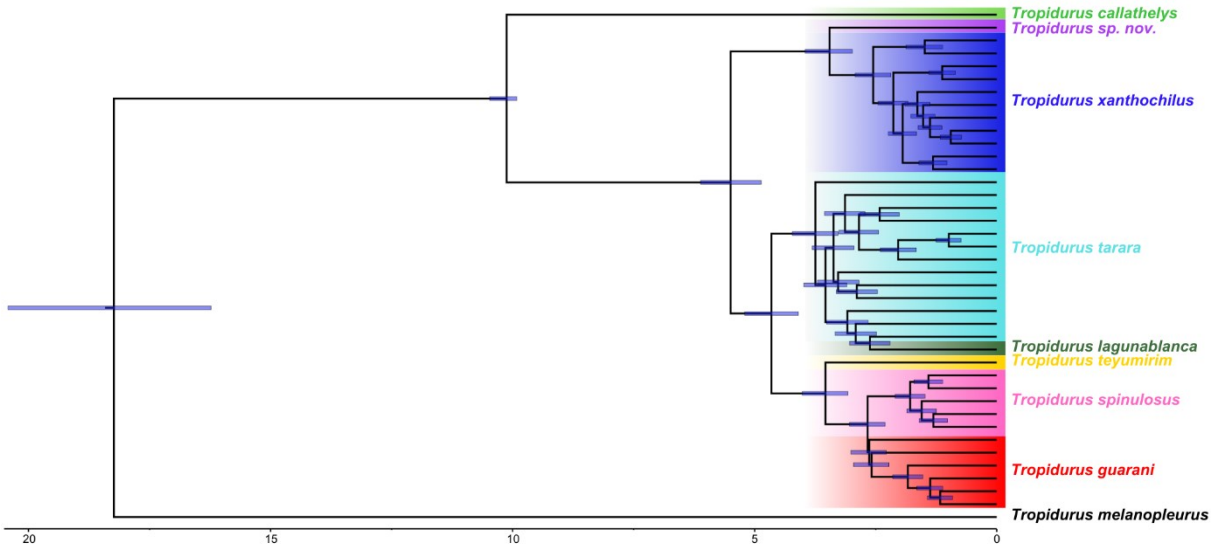

Fig. 2. Divergence times (Ma) estimated for the *Tropidurus spinulosus* species group using the UCE dataset. The 95% HPD interval of the posterior estimates (blue shaded bars), as estimated through the MCMCTree program, is shown above each node of the tree. The scale bar is in Ma. Specimen names are collapsed (for the fully detailed tree, see the Supplementary Material).

Phylogenetic networks and gene flow

We evaluated the potential for reticulate evolution in our dataset using five different approaches: (i) the phylogenetic networks applying quartets (SNaQ) method implemented in PhyloNetworks (Solís-Lemus and Ané 2016; Solís-Lemus et al. 2017); (ii) the maximum pseudolikelihood estimate (MPL) method implemented in PhyloNet (Wen et al. 2018); (iii) the extension of the typical tree-based model to general networks, assuming no ILS and independent loci, available in the NetRAX program (Lutteropp et al. 2022); (iv) ABBA-BABA tests for detecting gene flow between pairs of species, through the D-suite program (Malinsky et al., 2021); and (v) the MSC-M model implemented in BPP v.4.6 (Flouri et al. 2018; 2023) to estimate migration rate between pair of species that showed signals of mitonuclear discordance. The first four methods serve as exploratory tools to identify potential reticulations or gene flow events, while the BPP-based approach directly quantifies migration rates.

Analyses of the UCE dataset using PhyloNetworks revealed that models incorporating up to three reticulation events provided a better fit to our data compared to strictly bifurcating

210 trees, where gene tree discordance is attributed solely to ILS. However, these events are
211 mostly intraspecific and do not involve the species with discordant relationships, thus
212 Phylonetworks does not indicate that reticulation is the main source of mitonuclear
213 discordance (Supplementary Figures S12-S15; Table S1). Analyses using the other
214 phylogenetic network approaches corroborated the pattern of minimal reticulations between
215 species observed in our UCE data (Supplementary Figures S16-S18), and D-suite tests
216 (Malinsky et al., 2021) for detecting gene flow also do not indicate significant nuclear
217 admixture within the *Tropidurus spinulosus* species group (Supplementary Table S2). Please
218 refer to the Supplementary Material, section "*Details on Phylogenetic Networks methodology*
219 *and results*," for a detailed explanation on all reticulation tests.

220 Analyses in BPP under the MSC-M model with nuclear data—100 UCE loci (93,246 bp)
221 selected for clock-likeness using SortaDate (Smith et al. 2018)—indicates minimal or no gene
222 flow among extant species, but inclusion of ancestral populations yields higher migration rate
223 estimates (Figure 3; Supplementary Tables S3-S4), particularly those associated with the
224 observed phylogenetic discordance. This pattern is robust to the choice of different guide
225 trees: whether constrained by the mitochondrial topology or by the partitioned nuclear
226 topology, although the first produces relatively higher migration rate values. Notably, both
227 guide tree inferences implicate *Tropidurus xanthochilus*, or its ancestors, in these ancient gene
228 flow events, suggesting that historical mitochondrial capture involving this lineage may
229 underlie the main observed discordances between nuclear and mitochondrial phylogenies.
230 Also, when combining the nuclear dataset alongside the complete mitochondrial genome (100
231 UCE loci, 93,246 bp + 1 mitochondrial partition, 13,578 bp), higher rate estimates were
232 generally produced than those obtained using the nuclear dataset only. In this case, migration
233 rates using the combined dataset (with mitochondrial and nuclear partitions) were higher

234 than the estimates using solely the nuclear data (Table S4). In summary, across all migration
235 scenarios evaluated, including information derived from the mitochondrial data (whether
236 based on topology or mitogenome alignments) consistently resulted in higher inferred
237 migration rates compared to nuclear-only analyses, demonstrating that the inclusion of
238 mtDNA in the analysis strengthens the detection of historical gene flow in this system.

239

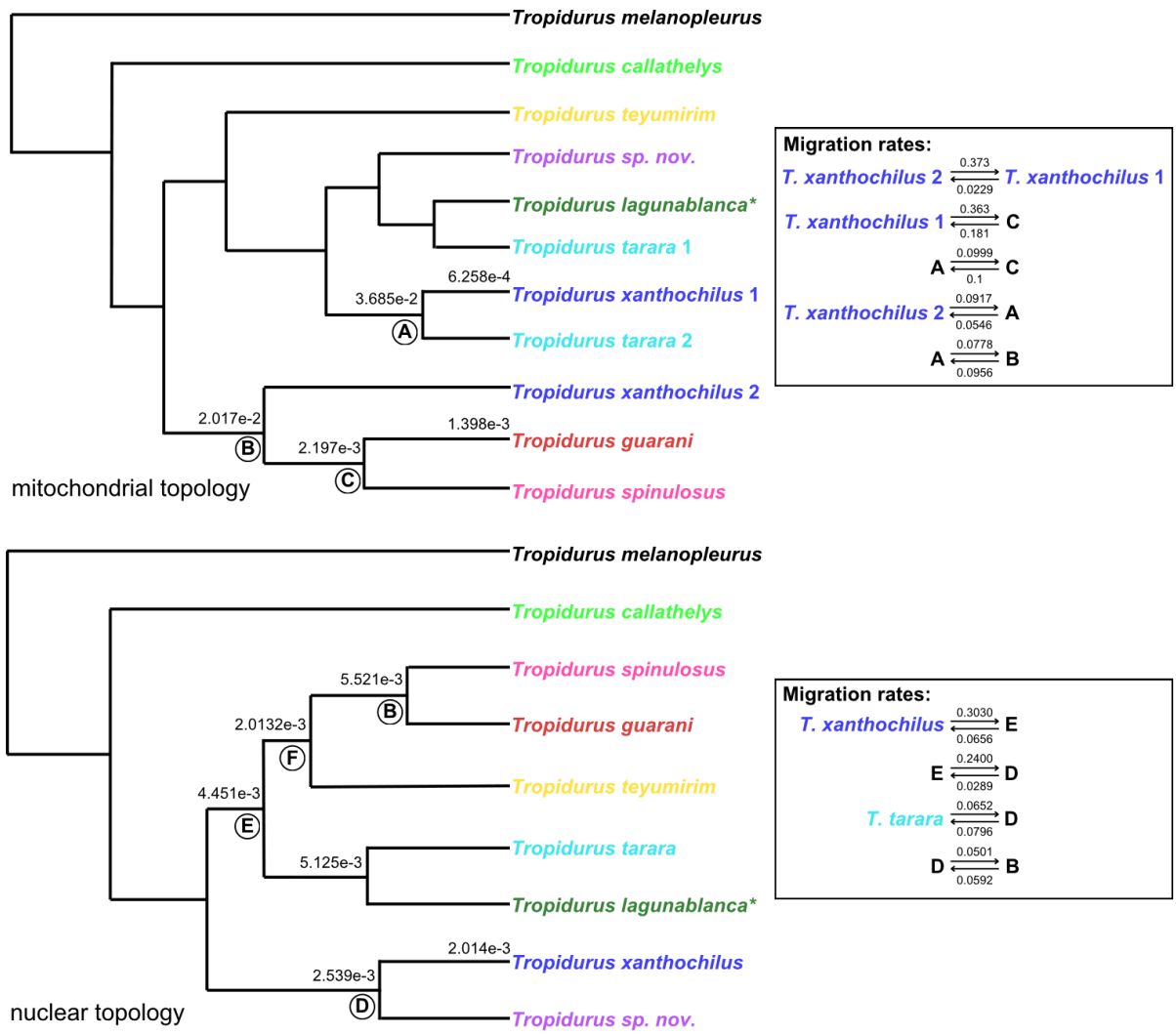

240
241 Fig. 3. Migration (MSC-M) model for *Tropidurus spinulosus* species, displaying only the scenarios with the highest
242 estimated migration rates. For a complete list of all tested migration scenarios and their corresponding rate
243 values, please refer to the Supplementary Material. Population size (theta, θ) values for each species or ancestral
244 node involved in gene flow events are shown above the branches, with the remaining theta values also provided
245 in the Supplementary Material. The upper panel presents the analysis using the mitochondrial topology as the
246 guide tree, whereas the lower panel shows the same analysis based on the nuclear topology, in this case using
247 both nuclear and mitochondrial data as input. In both trees, the circled letters below the nodes denote the
248 ancestral lineages included in the migration tests.
249

250 Estimates of population size (θ) for both current species and ancestral populations
251 further support the previously described scenario (Figure 3; Supplementary Tables S5-S6), for
252 instance indicating a directional gene flow event in which the larger ancestral population of
253 the *T. guarani* + *T. spinulosus* clade might have captured *T. xanthochilus* mitochondrial
254 genomes.
255
256 *Selection*
257 Regarding the mtDNA dataset, our analyses indicate minimal evidence of positive
258 selection acting on the mitogenomes of *Tropidurus spinulosus* lineages. Codon-based tests
259 detected limited signatures of episodic positive or diversifying selection: MEME (Mixed Effects
260 Model of Evolution; Murrell et al. 2012) identified nine sites (two in ATP6, one in ATP8, one in
261 COX1, two in COX2, and one in COX3) with p-values ≤ 0.05, while FUBAR (Fast, Unconstrained,
262 Bayesian AppRoximation; Murrel et al. 2013) detected two sites (one in COX1 and one in
263 COX2) with posterior probabilities ≥ 0.95. In contrast, both BUSTED (Branch-Site Unrestricted
264 Statistical Test for Episodic Diversification; Murrel et al. 2015) and aBSREL (adaptive Branch-
265 Site Random Effects Likelihood; Smith et al. 2015) analyses did not reveal significant episodic
266 selection along any branches in the mitogenomic phylogeny, even after formal testing of 36
267 branches with correction for multiple comparisons. Furthermore, we did not observe any
268 species with extreme nucleotide diversity (π) values, which could indicate selection on
269 mitochondrial lineages; instead, the diversity values were nearly identical across all
270 populations (Supplementary Table S7). Notably, the significantly negative Tajima's D (p ≤ 0.05,
271 Supplementary Table S8) indicates an excess of rare variants, a pattern that can arise from
272 both demographic expansion and selection. Subsequent analyses support a scenario of recent

273 expansion for the main populations, suggesting that this signal is evidence of historical
274 demographic changes rather than selection acting on the mitogenomes.
275
276 *Demographic history*
277 As previously demonstrated, BPP estimates of population size reveal differences
278 among ancestral populations likely involved in the ancient introgression events underlying the
279 observed discordance; these differences also support the inferred direction of gene flow
280 (please refer to the *Migration tests in BPP* section of the Supplementary Material as well).
281 Furthermore, our results indicate that demographic fluctuations (particularly rapid population
282 expansions) may have facilitated the fixation of mitochondrial haplotypes through neutral
283 processes such as genetic drift. These demographic shifts could also have diluted signatures
284 of introgression in the nuclear genome, even if such events occurred prior to the observed
285 population size changes detailed below.
286 Specifically, our Extended Bayesian Skyline Plots (EBSP; Heled and Drummond 2008)
287 revealed a pronounced increase in effective population size for all populations, particularly in
288 the last 100.000 years (Figure 4). Given that *Tropidurus tarara* was recovered in two distinct
289 clusters within the mitochondrial tree, we highlight that independent analyses were
290 conducted for each group. As results were identical across both groups, we present the EBSP
291 for only one cluster, which we consider representative of the species as a whole. For the
292 nuclear dataset, Stairway Plot analyses (Liu and Fu 2020) for *T. xanthochilus*, *T. tarara*, *T.*
293 *spinulosus*, and *T. guarani* revealed a consistent pattern across species, characterized by
294 population expansion mainly beginning 60,000 years ago, followed by relatively stable
295 population sizes thereafter (Figure 5). It is important to note that, since *T. guarani* was
296 recovered as paraphyletic in the nuclear phylogenetic analyses, we only considered samples

that consistently formed a clade, regardless of the analytical approach employed (see the Methods section for details).

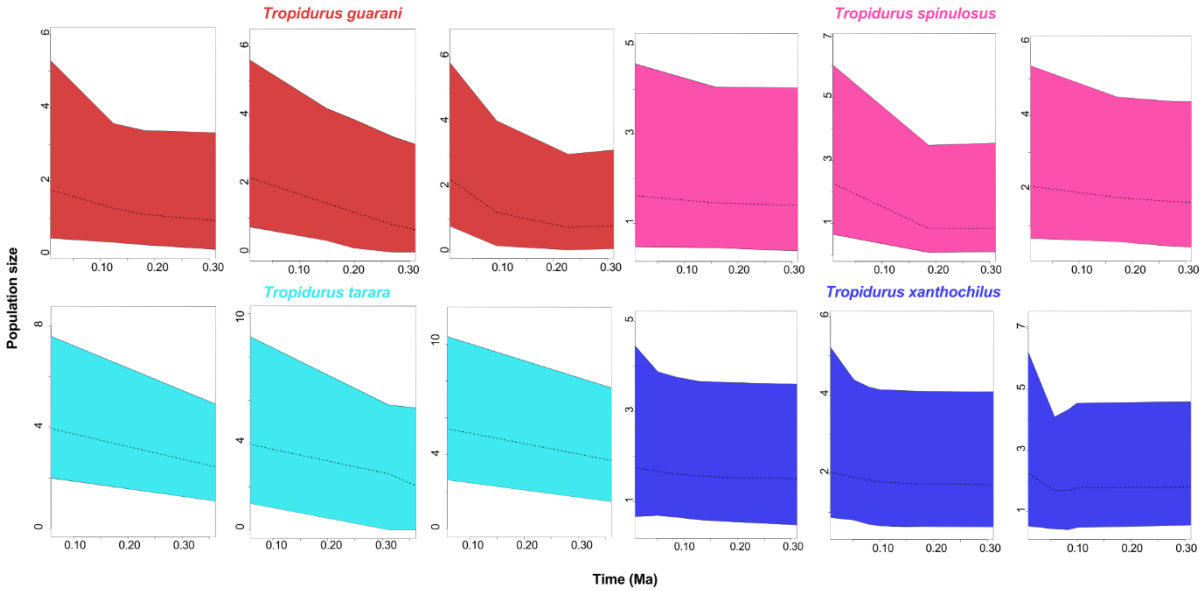

Fig. 4. EBSP results showing changes in effective population size through time for lineages in the *Tropidurus spinulosus* species group, based on three mitochondrial partitions (from left to right: cytb, 12 + 16s, and COX1, 2 and 3). Y-axis shows the effective population size with respective mean (dashed lines) and 95% HPD limits (the surrounding colored area delimited by the continuous lines). Assuming a generation time of 1 year, the current effective population size estimated at 1 would be equivalent to around 1 million. While this number appears large, it serves only as an illustration. Actual values will vary depending on the chosen mutation rate and generation time. The x-axis shows time in Ma as time goes backwards from left to right.

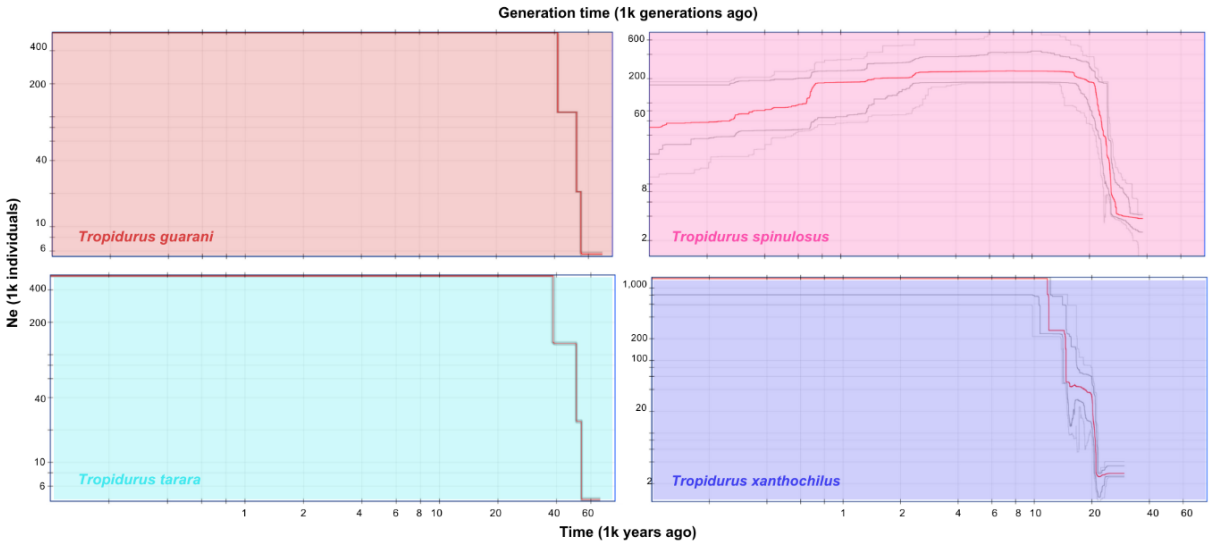

Fig. 5. Stairway Plot demographic inferences of four lineages within the *Tropidurus spinulosus* species group. The red line shows the median estimate of the effective population size (Ne). The gray lines indicate the 75% (dark) and 95% (light) confidence intervals.

Discussion

Our genomic analysis of the *Tropidurus spinulosus* species group reveals a complex evolutionary history characterized by: (a) significant discordance between nuclear and mitochondrial phylogenetic groupings, with very low levels of nuclear introgression; (b) at least two major mitochondrial capture events, specifically involving ancient *T. xanthochilus* populations and non-sister groups such as the *T. spinulosus* + *T. guarani* clade and *T. tarara*; (c) no signs of strong positive selection acting on mtDNA; and (d) demographic evidence of recent population expansions in both nuclear and mitochondrial genomes across various species in the group, along with differences in the sizes of ancestral populations that may have reinforced introgression events directionality. Given these findings, we suggest that the mitonuclear discordance observed in this study likely originated from admixture among ancient populations of the *T. spinulosus* species group that experienced long-term isolation, followed by secondary contact.

335 *Methodological challenges in investigating introgression as a cause of mitonuclear*
336 *discordance*

337 Some caution is warranted when interpreting our results, especially given the nature
338 of our dataset. UCEs, by definition, represent highly conserved genomic regions shared across
339 evolutionarily distant taxa (Faircloth et al. 2012). While this might suggest that such data are
340 primarily suited for addressing 'deep' phylogenetic questions, multiple studies have
341 demonstrated their utility at the population and individual levels (Smith et al. 2014; Raposo
342 do Amaral et al. 2018). Additionally, the introgression and gene flow tests we used are able to
343 capture events on different time scales. For instance, the ABBA-BABA test assumes that
344 multiple substitutions at a given site are rare, as an excess of substitutions can distort patterns
345 of site discordance. This assumption tends to break down in deeply divergent taxa (Hibbins
346 and Hahn 2022), making the ABBA-BABA test more suitable for detecting recent introgression
347 events. In our study, only one significant case of interspecific gene flow was detected (both in
348 the case of the PhyloNetworks analysis and the ABBA-BABA tests), though it warrants caution
349 (as discussed below). Conversely, phylogenetic networks, which analyze discordance between
350 gene trees and other concordant factors, are less impacted by multiple substitutions at
351 individual sites, which makes them better suited for detecting older introgression events
352 (Hibbins and Hahn 2022).

353 Therefore, as we used different methodologies capable of detecting signals across
354 distinct time scales, our results cannot be considered totally dependent on the nature of the
355 used markers—even considering that the accuracy of phylogenetic network methods may also
356 depend on the number of gene trees used. In this regard, previous studies have shown that a
357 similar number of gene trees compared to our dataset is sufficient to reliably recover an
358 accurate network topology, although the exact direction of reticulation events may remain

359 uncertain depending on the evolutionary scenario (Solís-Lemus and Ané 2016). Moreover, the
360 consistency of recovered topologies across multiple analyses, with varying levels of data
361 completeness, suggests that the majority of our UCE gene trees are not either unresolved or
362 phylogenetically uninformative. Therefore, although other genomic markers may offer
363 greater sensitivity for detecting introgression, the consistency of our results across multiple
364 analytical frameworks—each suited to detecting gene flow over different temporal scales—
365 supports the conclusion of minimal or no nuclear introgression within the *Tropidurus*
366 *spinulosus* group. In any case, future comparative studies are warranted to evaluate how the
367 choice of genomic markers may influence the detection of complex evolutionary processes
368 such as introgression.
369
370 *Decoupled histories: mitonuclear discordance with minimal nuclear introgression*
371 Reports of mitonuclear discordance are not unexpected, given that mitochondrial and
372 nuclear genomes evolve semi-independently. In this context, while previous studies have
373 documented nuclear introgression associated with mitonuclear discordance (e.g., Zieliński et
374 al. 2013; Myers et al. 2022), our findings suggest a different pattern. For instance, while we
375 identified one significant nuclear reticulation event involving *Tropidurus*
376 *callathelys* (Supplementary Figure S14) and one significant D-statistic result involving *T.*
377 *teyumirim* (Supplementary Table S2), these findings require cautious interpretation. First,
378 there is no evidence suggesting contemporary hybridization within the *T. spinulosus* group.
379 The known biology and distribution of these specific lineages do not suggest the occurrence
380 of hybridization events between them (Carvalho et al. 2013; Carvalho 2013; 2016), although
381 this may reflect a distinction between contemporary gene flow and the ability of our methods
382 to detect introgression over evolutionary timescales. Second, the extreme sampling disparity

383 (n=1 for both *T. teyumirim* and *T. callathelys* versus larger samples for other taxa) could have
384 contributed to false positives in ABBA-BABA tests, which have reduced sensitivity at low
385 admixture levels (Durand et al. 2011), and PhyloNetworks analyses due to stochastic effects.

386 ILS is another phenomenon that can contribute to mitonuclear discordance, and its
387 signals can easily be mistaken for those caused by introgression (Andersen et al. 2021; DeRaad
388 et al. 2023). In our case, if some samples of a species coalesced deep in the tree, before this
389 lineage diverged from its common ancestor, a significant portion should have coalesced if ILS
390 were the predominant factor driving the discordance with mitochondrial data. However, even
391 our phylogenetic network analyses explicitly accounting for ILS (particularly PhyloNetworks
392 and PhyloNet) did not detect substantial nuclear introgression events. Moreover, the
393 agreement between partitioned (based on IQ-TREE) and ASTRAL analyses of nuclear markers
394 also suggests that ILS has a limited impact on the phylogenetic signal (Supplementary Figures
395 S1-S6), as ASTRAL is designed to recover the correct topology even under high levels of ILS
396 (Zhang et al. 2018).

397 Finally, it is important to acknowledge the lack of methods specifically designed to
398 detect mitochondrial genome introgression with the same level of precision available for
399 nuclear markers. The approach adopted in this study—particularly the BPP-based framework
400 using both mitochondrial and nuclear topologies as guide trees and integrating the
401 mitochondrial partition with multiple nuclear loci (Figure 3)—was designed to illustrate how
402 gene flow may differ between nuclear and mitochondrial genomes due to their distinct
403 inheritance patterns and evolutionary dynamics. Furthermore, we also aimed at emphasizing
404 the value of a genome-wide analytical perspective for understanding the role of introgressive
405 hybridization in animal speciation—an approach still lacking in many biological systems (Good
406 et al. 2015).

407 By doing that, we discovered that while our nuclear data largely dismiss the occurrence
408 of prominent introgression within the *Tropidurus spinulosus* group, the mitochondrial genome
409 presents a contrasting picture. Migration rate estimates increase when mitochondrial DNA is
410 included—either as an additional partition or by using the mitochondrial topology as the guide
411 tree (Tables S3-S4). Specifically, while BPP analyses of 100 UCE loci produced minimal
412 migration rate estimates (under the nuclear-guided topology), incorporating the mitogenome
413 into the dataset increased the estimated values despite the much larger size of the nuclear
414 dataset. Importantly, higher migration rate estimates appeared only in scenarios involving
415 ancestral populations (regardless of whether the nuclear or mitochondrial topology was used
416 as the guide tree), producing more realistic values (Figure 3). These findings not only
417 underscore the analytical value of including mitochondrial data in gene flow estimates but
418 also support the conclusion that the nuclear phylogenies more accurately reflect species
419 history in the *T. spinulosus* system.
420
421 *Proximate explanations of mitonuclear discordance in the Tropidurus spinulosus species group*
422 Evidence supporting a demography-related hypothesis regarding introgression
423 typically falls into three main categories (e.g., Hinojosa et al. 2019; Palacios et al. 2023; Shen
424 et al. 2025): (i) prolonged periods of isolation; (ii) population growth leading to secondary
425 contact; and (iii) a biogeographic signal related to the discordance. Below, we discuss how our
426 findings align with this framework, as the primary cause of the mitonuclear discordance
427 reported in this study is mitochondrial capture associated with the demography of the
428 lineages within the *Tropidurus spinulosus* group. Specifically, our results indicate ancient gene
429 flow events occurring in populations that were likely isolated for extended periods before
430 undergoing secondary contact, although we detected limited evidence of nuclear

431 introgression. Additionally, both nuclear and mitochondrial datasets reveal widespread
432 historical fluctuations in population size (Figures 4 and 5). Similar cases have been
433 documented in lizards (e.g., Myers et al. 2022), where geographic isolation, followed by range
434 and demographic expansions, led to secondary contact and gene flow between previously
435 diverged groups.

436 First, our divergence time estimates support a gradual and prolonged separation
437 among species in the *Tropidurus spinulosus* group, with divergence events between species
438 occurring from 20 Ma onward. Specifically, the initial split occurred between 20 and 15 Ma,
439 with *T. melanopleurus* diverging first. Around 10 Ma, *T. callathelys* separated from the
440 remaining taxa, while most subsequent speciation events took place between 8 and 2.5 Ma
441 (Figure 2). Related to that, it is important to note that the evolutionary history of South
442 America's dry diagonal has been shaped by multiple Neogene (23 Ma onward) geological and
443 climatic processes, with individual taxa responding uniquely to local conditions (Guillory et al.
444 2024). Deep divergences among Squamates, including those within the *T. spinulosus* group,
445 likely stem from Miocene events such as the uplift of the Central Brazilian Plateau and marine
446 incursions in the southern dry diagonal (Guillory et al., 2024; Bezerra et al., 2025).

447 If such geological events led to prolonged geographic isolation of lineages, their
448 gradual cessation would have increased opportunities for secondary contact and potential
449 introgression, particularly when coupled with demographic and range expansions. In such a
450 scenario, periods of secondary contact may have led to the formation of hybrid zones with
451 varying levels of interbreeding, followed by contrasting patterns of gene flow between the
452 nuclear and mitochondrial genomes. During periods of geographic and/or demographic
453 expansion, nuclear genomes—subject to recombination and meiotic segregation—undergo
454 widespread admixture and tend to homogenize over time, diluting distinct traces of past

455 isolation and secondary contact. In contrast, divergent mitochondrial haplotypes, which are
456 non-recombining and inherited solely from the females, may persist due to genetic drift,
457 particularly if introgression occurred early in the population expansion or when the population
458 sizes were relatively low.

459 The directionality of gene flow events is another factor that could have played a crucial
460 role in facilitating neutral mitochondrial capture. Because genetic drift is more pronounced in
461 small populations, neutral mutations in mitogenomes are more likely to become fixed (Moore
462 1995; Després, 2019). Consequently, unidirectional introgression from a larger, resident
463 population into a smaller, invading one would be more probable during the early stages of
464 contact. If the ancestral populations of any of *Tropidurus spinulosus* species were more
465 restricted in distribution at that point, such conditions would further facilitate the fixation of
466 captured mitochondrial variants through drift. The repeated instances of discordance
467 involving *T. xanthochilus*, due to ancient introgression, may suggest that this lineage had a
468 smaller population size compared to others. Our ancestral population size estimates are
469 consistent with this scenario. For instance, in the model where migration rates are higher (in
470 this case, using the mitochondrial topology as the guide tree; Supplementary Tables S3-S4), Θ
471 estimates of *T. xanthochilus* are considerably lower than those of the ancestor involved in the
472 gene flow event—in this case M (*T. xanthochilus* → ancestor (*T. guarani*, *T. spinulosus*)) =
473 0.3629, with Θ values of 0.0006258 and 0.02017, respectively (Supplementary Table S5). A
474 similar pattern was observed when the nuclear topology was used as the guide tree, with the
475 ancestors of the *T. tarara* + *T. spinulosus* + *T. guarani* clade exhibiting higher Θ values than
476 those of the ancestral *T. xanthochilus* populations (Supplementary Table S6). Under this
477 scenario, it would be plausible to suggest that the mitogenomes of some *T. xanthochilus*

478 individuals could have been incorporated by the larger ancestral populations of the *T. guarani*
479 + *T. spinulosus* clade, and also by ancestral populations of *T. tarara*.

480 It is also noteworthy that our main demographic analyses (EBSP and Stairway Plot)
481 might have captured a shorter time scale than that over which the gene flow events occurred.
482 Even so, relatively recent demographic shifts, during the Pleistocene (2.5 Ma – 12 kya), may
483 have contributed to the discordance pattern as well, either by facilitating the fixation of
484 mitochondrial variants or reducing detectable signals of nuclear introgression. Population
485 expansion events, in particular, appear to have occurred from at least 100 kya onward (Figures
486 4 and 5), supporting this interpretation. Similar patterns of demographic fluctuation shaping
487 phylogeographic histories have been reported for other squamates as well (Guillory et al.
488 2024). Moreover, the observed differences in temporal estimates of species demography
489 between those two approaches (Figures 4 and 5) are likely attributable to the distinct
490 mutation rates we applied to the mitochondrial and nuclear datasets. As with many non-
491 model organisms, species-specific substitution rate estimates for *Tropidurus* are unavailable,
492 adding uncertainty to time-based inferences.

493 The two particular instances of mtDNA capture involving *Tropidurus xanthochilus* are
494 also associated with biogeographic signals: one possibly occurring to the west of *T.*
495 *xanthochilus*' distribution, involving ancestral populations of the *T. spinulosus + T. guarani*
496 clade, and another to the south, involving *T. tarara*. Broadly speaking, *T. spinulosus* is found
497 west of the Paraguay River, primarily within the Chaco region (Carvalho 2013). Specifically, its
498 distribution spans from north-central Argentina and northwestern Paraguay to southeastern
499 and central Bolivia, covering both the Chaco and dry forest zones (Frost et al. 1998; Carvalho
500 2013). Although distributional data remain limited, the known ranges of *T. spinulosus* and *T.*
501 *xanthochilus* are allopatric. The nearest known populations of *T. spinulosus* are located at least

350 km south of the type locality of *T. xanthochilus,* near to the '*Serranía de Huanchaca*' (Harvey and Gutberlet, 1998). Even so, Harvey and Gutberlet (1998) proposed that *T. xanthochilus* and *T. spinulosus* might be parapatric in the area where the forests of the Tarvo and Paraguá Rivers merge with the semideciduous *'Chiquitania'* dry forest. On the other hand, *T. tarara* is currently documented from locations in the northern portion of Eastern Paraguay, east of the Paraguay River, and its range extends into the Brazilian state of Mato Grosso do Sul (near the southern limit of the distribution of *T. xanthochilus*).

In this context, future studies—whether empirical or based on modelling scenarios—will be crucial to assess the potential overlap (past or present) in the distributions of *T. xanthochilus* with *T. spinulosus* + *T. guarani* clade, and *T. tarara* as well. Such overlap would provide additional biogeographical evidence for mitochondrial capture among these lineages. Environmental changes can increase opportunities for hybridization and introgression through neutral demographic processes (Excoffier et al. 2009; Phuong et al. 2016), with mitonuclear discordance of this nature often linked to climatic instability and its effects on demographic dynamics (Phuong et al. 2016). Phylogenetic niche modeling, which combines past and present climate data with occurrence records and time-calibrated phylogenies to reconstruct historical geographic ranges (e.g., Guillory and Brown, 2021), may be particularly useful for testing these hypotheses in the future.

Finally, our findings suggest that mitochondrial capture in the *Tropidurus spinulosus* group likely occurred during a period when the current lineages were not yet fully differentiated and still overlapped in both space and time. This interpretation is supported by our migration rate results, which show that the highest estimated values were associated with scenarios involving ancestral populations (Figure 3). Particularly, this aligns with the "gray zone of speciation" concept—a transitional phase where populations shift from widespread

526 admixture to complete genetic isolation (Roux et al. 2016; Burbrink et al. 2021), facilitated by
527 pre and/or post-zygotic barriers (Stankowski and Ravinet, 2021).
528
529 *Mitonuclear discordance beyond neutral processes: a case for natural selection?*
530 Our analyses did not reveal strong evidence of positive selection acting on the
531 mitochondrial genome of the *Tropidurus spinulosus* species group. Site-model tests across the
532 phylogeny identified only a few individual codons under selection, indicating that these
533 methods captured limited signals of episodic or pervasive positive selection acting on the
534 mitogenome. However, it is important to note that these approaches are designed to detect
535 selection at the level of specific codons or phylogenetic branches, rather than to assess the
536 rapid fixation of mitochondrial haplotypes following introgression (see the HyPhy
537 documentation for a detailed explanation). In such a scenario, an entire haplotype could be
538 fixed in a new species, a process that might not be directly detectable by the methods adopted
539 here.
540 Nonetheless, complementary analyses, including nucleotide diversity estimates and
541 Tajima's D test results, do not provide support for natural selection either. First, comparable
542 π levels across the lineages involved in the discordance (Table S7) are not indicative of
543 selective forces strongly acting on the mitogenomes of *Tropidurus spinulosus* species.
544 Similarly, the negative Tajima's D values (Table S8), while theoretically compatible with both
545 selection and population expansion, are here interpreted as indicative of historical
546 demographic changes in light of the additional evidence previously discussed. Furthermore,
547 in lizards—where mitochondrial function is less constrained by high metabolic demands
548 compared to endotherms (Chung and Schulte 2020)—the selective pressure for rapid fixation
549 of an introgressed mitogenome is likely lower. Nonetheless, while selective factors are unlikely

550 to be the primary drivers of mitonuclear discordance in *T. spinulosus* lineages, adaptive
551 explanations may be still underrepresented in the literature (e.g., Mao and Rossiter 2020),
552 which may partly reflect the inherent challenges in reliably detecting selection on mtDNA
553 (Bonnet et al. 2017).
554
555 *Sex-biased dispersal in Tropiduridae and its potential role in mitonuclear discordance*
556 Finally, future investigations could look further into the role of mitonuclear
557 incompatibilities and mating systems in explaining contrasting signals between nuDNA and
558 mtDNA. Asymmetries between sexes in mating behavior, offspring production, and dispersal
559 are well-known demographic factors contributing to mitonuclear discordance (Dessi et al.
560 2022). For example, in species where males exhibit greater dispersal, nuDNA is expected to
561 show higher genetic homogeneity across distant populations, as male-mediated gene flow
562 facilitates the spreading and mixing of their genetic material. Conversely, if females are more
563 philopatric (i.e., remain near their birthplace), mtDNA may display greater population
564 structure, preserving historical patterns of isolation. As a result, while nuDNA may indicate a
565 single, cohesive population over a broad geographic range, mtDNA could reveal distinct
566 subpopulations shaped by limited female dispersal. This process can lead to geographically
567 structured mitochondrial lineages that persist despite widespread nuclear gene flow (see
568 reviews in Toews and Brelsford 2012; Bonnet et al. 2017). Currently, empirical data on the
569 dispersal behavior of *Tropidurus* species are lacking. However, research on certain groups
570 closely related to Tropiduridae (e.g., Phrynosomatidae) suggest that females exhibit strong
571 philopatry and possibly territoriality, while males may disperse further from contact zones,
572 facilitating nuclear gene flow but limiting mitochondrial inheritance (Qi et al. 2013). Although
573 limited studies have been conducted on squamate reptiles, some evidence indicates that sex-

biased differences in behavior and fitness can influence dispersal patterns. Therefore, we recommend future research to investigate whether sex-related dispersal contributes to the mitonuclear discordance observed in *Tropidurus*.

Conclusion

The growing number of reports documenting deep mitochondrial lineages without corresponding nuclear differentiation highlights the need for comprehensive molecular analyses, ideally employing phylogenomic approaches that incorporate both mitochondrial and nuclear markers. This is especially relevant for large genomic datasets, which can provide robust branch support, while also obscuring discordance among individual markers. Thus, integrative approaches are crucial for disentangling complex evolutionary processes that cause mitonuclear discordance, such as introgression, and for highlighting the unique role of mtDNA in detecting gene flow events that may be overlooked in nuclear data.

In this study, we explored a biological system where mitochondrial capture events were detected, offering insights and a foundation for future research into the evolutionary mechanisms underlying these patterns in Neotropical squamates. By analyzing different types of genetic markers, we provided a thorough investigation that contributes to the understanding of the complex evolutionary history of the *Tropidurus spinulosus* species group. Beyond mapping a clear case of mitonuclear discordance, we suggest that certain mitochondrial genomes within this group have undergone ancestral introgression, likely followed by complete capture during secondary contact events. These events left minimal traces in the nuclear genome, due to the species' historical demography. Accurately quantifying these patterns and understanding their underlying mechanisms are crucial for a deeper comprehension of speciation processes.

598

599 **Methods**

600 *Sampling and Lab work*

601 The phylogenomic approaches used in this study were based on anchored sequencing
602 methods, specifically Ultraconserved Elements (UCE) as described by Faircloth et al. (2012).
603 We sequenced a total of 43 individuals (Supplementary Material, Table S9), representing all
604 species of the *Tropidurus spinulosus* group. RAPiD Genomics LLC (Gainesville, FL) was tasked
605 with sample library preparation and target enrichment of UCEs using the tetrapod 5k probe
606 set (Faircloth et al. 2012), followed by multiplexed paired-end (PE) sequencing (2 × 100 bp) of
607 UCEs on an Illumina HiSeq 3000 PE100 platform. Our samples are mainly distributed around
608 the Pantanal Basin, with some extending to dry environments of Paraguay and Argentina
609 (Figure 6).

610

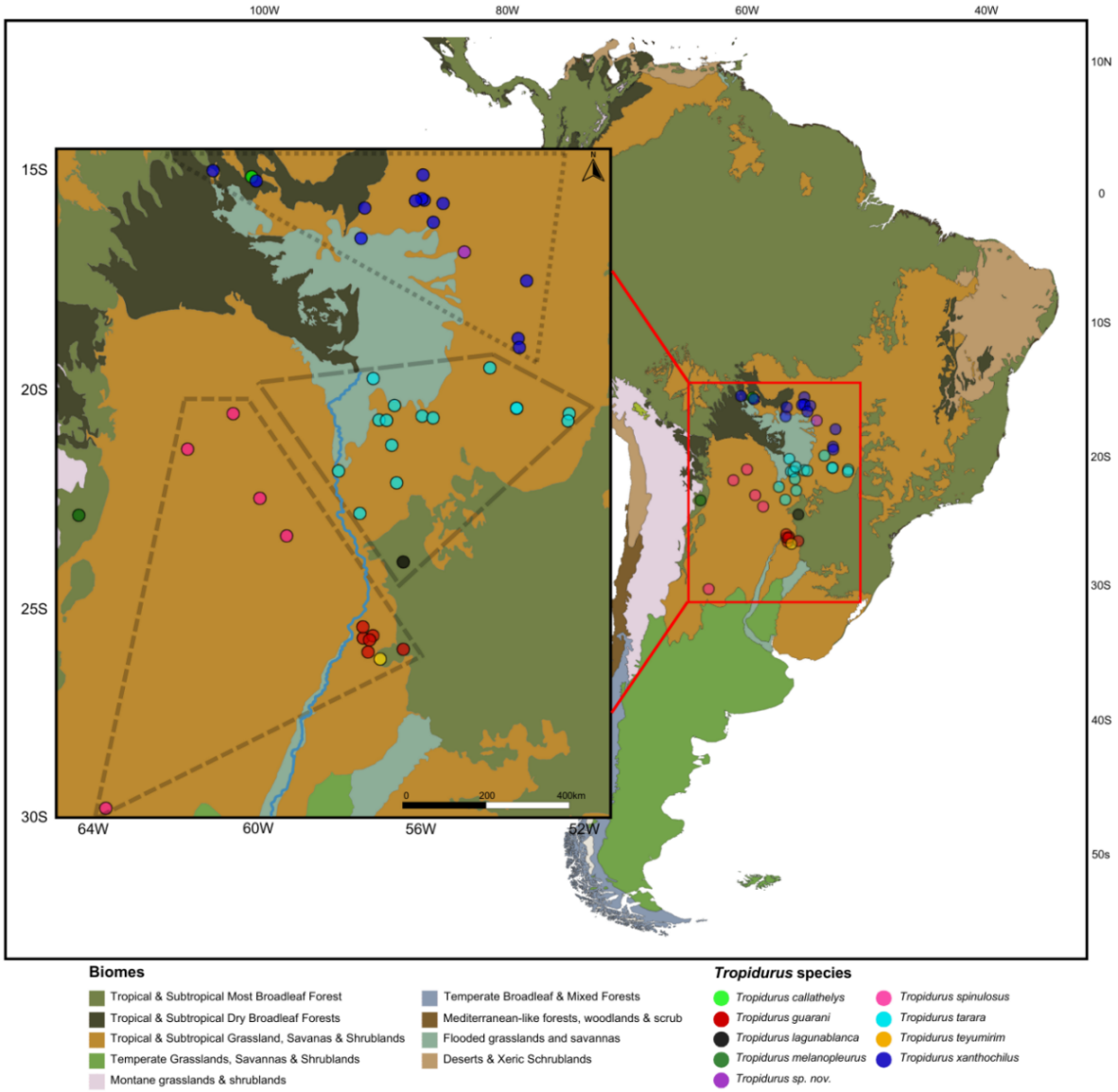

Fig. 6. Sample distribution with species assignments based on our concatenated phylogenetic analysis. The map at a larger scale shows the distribution of samples across various South American biomes, according to the classification of "Terrestrial Ecoregions of the World" adopted by the World Wildlife Fund. For a detailed review of the resolution and delimitation differences in these ecoregions, see Olson et al. (2001). The smaller-scale map highlights the specific region where the analyzed samples are distributed. Phylogenetically identified groups are marked with three distinct dashed line patterns, emphasizing their allopatric distribution: (1) the *T. spinulosus* + *T. guarani* + *T. teyumirim clade* (multi-species), (2) the *T. tarara clade* (with *T. lagunablanca* tentatively considered a synonym of *T. tarara*), and (3) the *T. xanthochilus* + *T. sp. nov.* clade. The map on the smaller box also shows part of the course of the Paraguay River (light blue), which separates the *T. spinulosus* lineages to the west from *T. guarani* and *T. tarara* to the east.

UCEs and mtDNA pipeline

We assembled the reads using the Phyluce v1.7.1 pipeline (Faircloth 2016). Demultiplexed reads were cleaned to remove low quality bases and adapter sequences in

629 Trimmomatic (Bolger et al. 2014), using the wrapper program illumiprocessor in Phyluce. To
630 accelerate assembly and render difficult datasets tractable, we normalized read depth at a
631 minimum of 5 using the script bbnorm.sh available in the BBTools suite (Bushnell 2018).
632 Trimmed and normalized reads were inspected for quality and adapter contamination using
633 FastQC v0.11.9 (Andrews 2010), and then assembled into contigs with SPAdes v3.15.5
634 (Bankevich et al. 2012). We used Phyluce to align assembled contigs back to their associated
635 UCE loci, remove duplicate matches, create a taxon-specific database of contig-to-UCE
636 matches and extract UCE loci for all individuals. Specifically, contigs matching UCE loci were
637 identified and extracted using the program LastZ v1.0 (Harris 2007) within Phyluce, both in
638 incomplete and complete (75% and 95% of completeness) matrices (see Faircloth 2016). After
639 probes and UCEs were matched, we aligned UCE contigs with MAFFT v7.471 (Katoh and
640 Standley 2013) using specific customized settings (-globalpair, --maxiterate 1000, --
641 adjustdirection), and trimmed the resulting alignments using the internal-trimming algorithm
642 (Gblocks: Castresana 2000). As a final step, AMAS (Borowiec 2016) was used to compute final
643 summary statistics for all alignments.

644 Due to the high abundance of mtDNA in samples and the less-than-perfect efficiency
645 of target enrichment methods, mitochondrial data, including entire mitogenomes are often
646 generated as a byproduct of the UCE sequencing process (Allio et al. 2020). Thus, we extracted
647 mtDNA from our contig assembly produced through Phyluce using MitoFinder (Allio et al.
648 2020), which can find and extract multiple mitochondrial genes or even entire mitogenomes
649 from assembled sets of bulk sequences. In general terms, the same alignment process
650 described above for UCEs was adopted for mitochondrial data.

651

652 *SNP calling workflow*

653 We selected the sample with the largest number of UCE loci among all individuals
654 ('MTR 29586', with 4800 loci) retrieved during the extraction step described above as the main
655 reference during the process of calling single nucleotide polymorphisms (SNPs), as
656 recommended in the Zarza et. al. (2016) pipeline to extract SNPs from UCE reads. Then, we
657 followed the sequence capture data from population-level samples workflow developed by
658 Harvey et al. (2016). The first step involves BWA, which was used to map raw reads from
659 individuals to contigs (Li et al. 2009; Li 2013). Thus, SAM files were converted to BAM with
660 SAMtools (Li et al. 2009). Alignments were checked for BAM format violations, read group
661 header information was added, and PCR duplicates were marked for each individual using
662 Picard (v. 1.106). The resulting BAM files for each individual in a lineage were merged into a
663 single file with Picard, which was then indexed with SAMtools. The Genome Analysis Toolkit
664 (GATK; v. 3.4-0; McKenna et al. 2010) was used to locate and realign around indels, which was
665 followed by calling SNPs using the 'UnifiedGenotyper' tool in GATK. SNPs and indels were then
666 annotated and indels were masked. Finally, we used GATK to restrict our datasets to high-
667 quality SNPs (Q30 filter) and performed read-backed phasing. After that, we used the R
668 packages SNPfiltR (DeRaad 2022) and vcfR (Knaus and Grunwald 2017) to visual and iteratively
669 filter our SNP dataset based on specific quality and completeness metrics. For analyses
670 requiring unlinked SNPs, a linkage disequilibrium-based filtering approach was applied using
671 PLINK (Purcell et al. 2007) with fixed parameters (--indep-pairwise 50 10 0.5). At the end of
672 this process, two datasets were generated. The first, referred to as the '*unlinked SNP dataset*
673 *I*', included 42 samples and excluded the *Tropidurus melanopleurus* sample, retaining only one
674 sample external to the largest clade within the group, namely *T. callathelys* (used in D-suite
675 analysis; 40,265 SNPs, 25.34% missing data). The second one, '*unlinked SNP dataset II',* with
676 37 samples, excluding the *T. melanopleurus, T. callathelys, T. teyumirim* and *T. sp. nov.*

677 samples, and assigning the *T. lagunablanca* sample as *T. tarara* (used in Stairway Plot analysis;
678 27,454 SNPs, 24.71 % missing data).
679
680 *Gene and species tree analysis*
681 Gene trees for all UCE loci and the mtDNA locus were inferred using IQ-TREE v2.2.6
682 (Minh et al. 2020), and support was inferred using 1000 ultrafast bootstraps (≥ 95 considered
683 as strong support). For partitioned ML analyses, ModelFinder (Kalyaanamoorthy et al. 2017),
684 part of the IQ-TREE package, was used to select the best fit model for each partition followed
685 by tree reconstruction (-m TESTNEWMERGE option), allowing partitions to have different
686 evolutionary rates (-spp option). Support was inferred using 1000 ultrafast bootstraps.
687 Additionally, species trees were inferred for the UCE dataset using ASTRAL v5.15.4 (Zhang et
688 al. 2018), which does this from gene trees and provides internal branch lengths in coalescent
689 units of gene tree discordance, as well as branch support values in the form of local posterior
690 probabilities (LPPs). In our ASTRAL analyses, we used the topology resulting from the
691 partitioned approach produced through IQ-TREE as a reference. Finally, we used BPP v.4.6
692 (Flouri et al., 2018) to estimate a species tree for the *Tropidurus spinulosus* group, based on
693 the full dataset of 820 UCE loci.
694 In the case of mitochondrial data, besides partitioning by gene, the alignment was also
695 partitioned by third codon positions (in the case of coding sequences), and we did an
696 additional analysis including two outgroup species to evaluate the monophyly of the
697 *Tropidurus spinulosus* group — *Plica plica* and *T. torquatus* (Supplementary Figure S6;
698 GenBank accession numbers: AB218961 for *P. plica*, and KU245273, KU245300, KU245090 and
699 KU245062 for *T. torquatus*). We present only the trees (both based on nuDNA and mtDNA)
700 featuring species from the *T. spinulosus* group (our in-group) in the results section. In all cases,

701 trees were manually rooted in *T. melanopleurus* using FigTree (Rambaut 2014), following the
702 topology obtained in the previously described analysis.
703
704 *Divergence time estimation*
705 A time-tree was inferred using two different approaches. The first one was the
706 RelTime-Branch Lengths method (Tamura et al. 2018), available in MEGA11 (Tamura et al.
707 2021), which uses a phylogenetic tree previously estimated branch lengths to infer divergence
708 dates. In this case, the time-tree was computed using the UCE-based phylogenetic tree
709 (complete matrix) with one calibration constraint, namely the node separating *Tropidurus*
710 *callathelys* from all the other species in the group (and using *T. melanopleurus* as the
711 outgroup). We used 10.74 Ma as the reference value for this constraint following the
712 estimates obtained by Zheng and Wiens (2016) regarding the node separating *T. callathelys*
713 and the rest of the species in our ingroup. The method described in Tao et al. (2020) was used
714 to estimate confidence intervals and set a normal distribution on the node for which
715 calibration densities were provided, and a normal distribution was used with the mean
716 centered on 10.74 and standard deviation = 0.5.
717 Alternatively, divergence time estimates were also estimated using the MCMCTree
718 v4.10 program (dos Reis and Yang 2019), which uses an approximate likelihood calculation
719 approach. In this case, the 100 most clocklike UCE loci within our dataset were selected,
720 particularly the loci with the least root-to-tip variance. Clock-likeness was assessed using the
721 program SortaDate (Smith et al. 2018), which measures root-to-tip variance within gene trees
722 and then sorts them from highest to lowest variance. The calibration in this case was
723 performed by constraining the age of the same node described above by > 10 and < 11 Ma,
724 using a fixed topology. Molecular clock estimates were obtained using the independent rates

725 model and we used the HKY85 model. The gamma prior on the mean substitution rate for
726 partitions (rgene_gamma) was set to G (7, 9.75), which means a substitution rate of
727 approximately 0.00717 substitutions/site/Ma (value available for the phylogenetically closest
728 species to *Tropidurus* in the germline mutation rate study of Bergeron et al. 2023). The gamma
729 rate variance (sigma2_gamma) was specified with G (1, 10). Two independent runs were
730 performed, each consisting of 550.000 MCMC iterations, with 10.000 as burn-in, 'nsample' =
731 100.000, and 'sampfreq' = 5. The ESS of the MCMCTree runs were examined in Tracer v.1.7
732 (Rambaut et al. 2018) to determine convergence, and values > 200 were retained.
733
734 *Gene flow and phylogenetic network estimation*
735 Failing to consider the potential influence of gene flow and introgressive hybridization
736 among species can negatively impact phylogenetic inference (e.g. Solís-Lemus and Ané 2016;
737 Solís-Lemus et al. 2016). Therefore, given the mitonuclear discordance observed in the
738 *Tropidurus spinulosus* clade, we evaluated reticulate evolution using five approaches: three
739 phylogenetic network methods, ABBA-BABA tests, and migration rate estimates.
740 Regarding the network approaches, we first used the PhyloNetworks program (Solís-
741 Lemus et al. 2017), in which the inference of phylogenetic networks is done with maximum
742 pseudolikelihood from gene trees or multi-locus sequences (SNaQ; Solís-Lemus and Ané
743 2016). We supplied SNaQ with unrooted gene trees from 820 UCE loci containing
744 representatives for 32 focal samples; tests were also carried out with 23 and 30 samples, in
745 order to verify the possible influence of the number of tips on the estimation of reticulation
746 events. In all of these alternative tests, we did not use all 43 samples from the UCEs dataset
747 in order to lighten the computational load of the analyses. As results were similar in all
748 configurations, here we only report the estimates with 32 and 30 samples (Supplementary

749 Figures S13 and S14). Observed concordance factors (CFs) were calculated from the final 820
750 gene trees dataset (complete matrix, see previous section) and used to infer phylogenetic
751 networks with different maximum numbers of reticulation events (*hmax* up to 12, using 5
752 independent runs per h-value) and the proportion (γ) of genomic ancestry in the hybrid
753 lineage contributed by each parental species/lineage. As the default setting for SNaQ
754 considers that each allele in a gene tree corresponds to a specific tip in the network, we also
755 estimated a species-level network, in which each allele/individual was mapped to a particular
756 species, with the assignment done according to the patterns identified through IQ-TREE's
757 partitioned approach. In both cases, we performed a goodness-of-fit test to check whether a
758 given network could explain the quartet concordance factor data adequately (Cai and Ane
759 2021).

760 For the PhyloNet analysis (Wen et al. 2018), we applied the MPL algorithm to infer the
761 network assigning the maximum number of reticulations from 0 to 5, with 10 runs for each
762 reticulation value. We used the '-a taxa map' option to associate taxa with species in the
763 species tree, also following the patterns identified through IQ-TREE's partitioned approach. In
764 this case all individuals present the 820 UCE loci dataset were included in the analysis, but
765 using rooted gene trees (using *Tropidurus melanopleurus* as the outgroup). In both
766 PhyloNetworks and PhyloNet analyses, support for each value of *h* (number of hybridization
767 events) was evaluated using the graphical slope heuristic, which involves plotting the
768 pseudolikelihood scores against *h* (referred to as *hmax*), following the framework proposed
769 by Solís-Lemus et al. (2017). Finally, the same dataset used for PhyloNetworks was also used
770 in the NetRAX program (Lutteropp et al. 2022), but the input of NetRAX is the partitioned
771 alignment itself, not the gene trees.

772 We used D-suite (Malinsky et al. 2021) as a complementary analysis to get gene flow
773 estimates obtained from Patterson's D and f-4 ratio analyses between populations/species. In
774 this approach, ABBA-BABA proportions were obtained with the Dtrios' program for all samples
775 in the *unlinked SNP dataset I,* and applying different assignment configurations of samples to
776 populations/species (Table S10). This program fixes the outgroup and then estimates ABBA-
777 BABA in all possible combinations of three populations. For example, in a tree with four
778 branches plus a fixed outgroup, Dtrios estimates four independent ABBA-BABA by excluding
779 one of the populations at a time, and assigning the remaining three populations as P1, P2, and
780 P3. Moreover, regarding ABBA-BABA positions, in D-suite P1 and P2 are ordered so that nABBA
781 ≥ nBABA and the resultant D statistic is always positive. Therefore, all the results, including
782 the f4-ratio and other statistics reflect evidence of excess allele sharing between P3 and P2
783 for each trio. Additionally, when testing for introgression among highly divergent species or
784 for ancient introgression events, the D-statistic might indicate false signals of introgression
785 due to substitution rate variation among branches. To address this issue, we used the '--
786 ABBAclustering' option available in the D-suite program, where greater clustering of sites
787 would indicate a real gene flow event rather than a false positive caused by homoplasy.
788 As a final approach to assess how gene flow differentially impacted nuclear and
789 mitochondrial genomes, we used the migration model (MSC-M) available in BPP v.4.6 (Flouri
790 et al. 2018; 2023). This allowed us to estimate the number of migrants per generation and the
791 direction of gene flow for species showing the strongest mitonuclear discordance in our
792 phylogenetic trees. This was done in two stages, either using the nuclear species tree or the
793 mitochondrial genealogy as the guide tree. In the first case, we used only a portion of the
794 nuDNA dataset—specifically, the 100 most clocklike UCEs (as previously described). A second
795 migration analysis was performed using that same dataset, but this time incorporating

796 mitochondrial data alongside nuclear data. In other words, two analyses were conducted
797 using the nuclear topology as the guide tree: one using nuclear markers only (100 UCE loci,
798 93,246 bp) and another combining nuclear data with mitochondrial data (100 UCE loci, 93,246
799 bp + 1 mitochondrial partition, 13,578 bp).

800 In both cases we tested bidirectional migration scenarios with the following species:
801 *Tropidurus xantochilus* ↔ *T. guarani*, *T. xanthochilus* ↔ *T. spinulosus,* and *T. xanthochilus* ↔ *T.*
802 *tarara*. Scenarios involving ancestral populations or species of the following groups were also
803 tested. For analyses using the mitochondrial genealogy as the guide tree, these included: (A)
804 *T. tarara* and one *T. xanthochilus* group; (B) *T. guarani* and *T. spinulosus*; (C) *T. guarani, T.*
805 *spinulosus* and another *T. xanthochilus* group. When using the nuclear topology as the guide
806 tree, the same scenarios with current species mentioned above were tested, while also
807 considering the following scenarios involving ancestral nodes: (B) *T. guarani* and *T. spinulosus*;
808 (D) *T. sp. nov.* and *T. xanthochilus*; (E) *T. tarara, T. guarani*, *T. spinulosus* and *T. teyumirim*; (F)
809 *T. guarani*, *T. spinulosus* and *T. teyumirim.* Population sizes (θ) were also estimated and
810 recorded for each species and ancestral node involved in the migration pairs. In all cases, we
811 used an inverse gamma prior of G(3, 0.04) for the Θ parameter and G(3, 0.2) for the τ
812 parameter, fixing the species model prior on the topologies described above. The gamma
813 migration prior used was 0.1 (α = 1, β = 10). We ran analyses for 4 x 10^5 MCMC generations,
814 taking samples every five and using 5 x 10^3 burn-in generations. To check for consistency of
815 results, we conducted two independent runs for each analysis.

816 Furthermore, we also used POPART v. 1.7 (Leigh et al. 2015) to generate a TCS
817 haplotype network (Clement et al. 2002), based on 3 mitochondrial genes - cytochrome c
818 oxidase I, II, and III (COX1, COX2, and COX3).

819

820 *Tests for positive selection and demographic changes through time*

821 To detect significant deviations from the hypothesis of neutral evolution in the mtDNA
822 dataset, we tested for the evidence of positive selection using MEME (Mixed Effects Model of
823 Evolution; Murrell et al. 2012), BUSTED (Branch-Site Unrestricted Statistical Test for Episodic
824 Diversification; Murrell et al. 2015), aBSREL (adaptive Branch-Site Random Effects Likelihood;
825 Smith et al. 2015), and FUBAR (Fast, Unconstrained, Bayesian Approximation; Murrell et al.
826 2013). MEME is designed to identify sites underlying episodic selection, BUSTED provides a
827 gene-wide (not site-specific) test for positive selection by asking whether a gene has
828 experienced positive selection at least one site on at least one branch, aBSREL focuses on tree
829 branches and can be used to test if positive selection has occurred on a proportion of
830 branches, while FUBAR uses a Bayesian approach to infer nonsynonymous (dN) and
831 synonymous (dS) substitution rates on a per-site basis for a given coding alignment and
832 corresponding phylogeny. All of these tests were performed utilizing the HYPHY package
833 through the DataMonkey server, using default parameters, and the threshold of $p < 0.05$ for
834 all four analyses. The same alignment of mitochondrial genes used for the phylogenetic
835 analyses was utilized here, with the particularity that in order to perform the selection
836 analyses, stop codons of each coding gene were removed, manually. Besides, Tajima's D was
837 calculated to evaluate evidence of natural selection and population size changes in the
838 mitogenome using the R function 'tajima.test', from the 'pegas' package (Paradis 2010).
839 Mitochondrial nucleotide diversity was estimated for populations of *T. guarani*, *T. spinulosus*,
840 *T. tarara*, and *T. xanthochilus* using the 'nuc.div' function, also from the 'pegas' package.

841 Because selection tests indicated neutrality in the mtDNA dataset (see results), we
842 then performed the multilocus coalescent-based EBSP (Heled and Drummond 2008)
843 implemented in BEAST v2.7.6 (Bouckaert et al. 2019) to estimate changes in effective

844 population sizes over time. Four phylogenetic groups were used in this analysis, namely:
845 *Tropidurus guarani*, *T. spinulosus*, one *T. tarara* clade and *T. xanthochilus*. Regarding this, we
846 highlight that demographic analyses typically assume that each analyzed group is
847 monophyletic and below the species level. While *T. guarani* is consistently recovered as
848 paraphyletic in our nuclear phylogenies, it forms a monophyletic clade sister to *T. spinulosus*
849 in mitochondrial analyses. Therefore, for the EBSP analysis, which was performed exclusively
850 with mitochondrial data, *T. guarani* was treated as a single lineage. A similar issue arises with
851 *T. tarara*, which appears as two distinct mitochondrial groups. In this case, analyses were
852 conducted separately for each cluster, but since the results were identical, only one is
853 presented in the text, as it effectively represents both *T. tarara* groupings. In the remaining
854 cases, samples were divided according to the clades recovered in the mtDNA partitioned
855 approaches previously described.

856 To reduce computational burden and facilitate convergence, we conducted separate
857 analyses on three sets of mitochondrial genes rather than using the entire mitochondrial
858 genome. These sets included: 1) cytochrome b (cytb); 2) COX1, COX2, and COX3; 3) 12S and
859 16S ribosomal RNAs. For coding gene analyses, alignments were partitioned by gene and
860 codon position, with tree and clock models linked across all partitions. Site models were
861 treated independently, with BEAST Model Test performed separately for each partition to
862 estimate mutation rates, and restricting potential models to the "namedExtended" set.
863 Regarding substitution rates, we set 1.0×10^{-2} as the mean for the COX partition, 6.339×10^{-3}
864 for the 12s + 16s partition, and 1.94×10^{-2} for the cytb partition, all reference values already
865 used in previous studies which used similar approaches when dealing with *Tropidurus'* mtDNA
866 in BEAST (e.g., Werneck et al. 2015; Camurugi et al. 2022; Carvalho et al. 2024). An
867 uncorrelated relaxed molecular clock was adopted in all three cases (with a normal

868 distribution for the 'ucldMean'; Sigma = 0.0025). Because the default of the hyper-prior of the
869 mean of the population size distribution ("populationMean.alltrees") is a sensitive option and
870 takes a long time to converge (requiring longer runs), we modified the prior to a Normal
871 distribution centered on 1.0 (Mean) with a standard deviation of 0.1 (Sigma) to improve
872 convergence. Initial tests were carried out to determine the optimum number of MCMC
873 simulations required for each of the populations. In most tests, we ran 500,000,000 MCMC
874 simulations, sampled every 50,000 chains. In all cases, three independent runs were carried
875 out and we checked for convergence using Tracer 1.7 (Rambaut et al. 2018) by visually
876 checking effective sample size (ESS > 200). In specific cases where convergence was not
877 achieved with this number of simulations, we combined logs with LogCombiner (Rambaut and
878 Drummond 2014) and used those files to generate EBSP plots.

879 To infer the demographic history using the nuDNA dataset, we first generated a folded
880 SFS file for the SNP dataset with easySFS (Gutenkunst et al. 2009). We then used Stairway Plot
881 v. 2.18 (Liu and Fu 2020) to estimate historical effective population size changes of *Tropidurus*
882 *xanthochilus*, *T. tarara*, *T. spinulosus* and *T. guarani*. For this last group, only the 4 samples
883 that form a clade in the partitioned phylogenetic analyses described above were used
884 (Supplementary Figures S1-S6). The parameters for the Stairway Plot analysis were as follows:
885 67% for the training sites, and one year was assumed as generation time (A. Carvalho, pers.
886 commun.). The nuclear mutation rate was assumed to be 7.17×10^{-9}
887 substitutions/site/generation, which is the value available for the phylogenetically closest
888 species to *Tropidurus* in the germline mutation rate study of Bergeron et al. (2023).

889 Table 1 provides a summary of all analyses conducted in this study, along with their
890 respective objectives and main results.

891 Table 1. Overview of the analytical workflow used in this study, detailing the rationale behind each step. SNP = single nucleotide
892 polymorphism; MSA = multiple sequence alignment; nuc = nuclear; mt = mitochondrial.

Method	Data	Analysis	Objectives	Main results
IQ-TREE	MSA-nuc (100, 95 and 75% UCE matrices) MSA-mt (coding + non-coding regions)	Individual-level phylogenies	What are the phylogenetic relationships of sampled individuals? Do nuc and mt topologies agree?	nuc: Three main clades detected: (*Tropidurus xanthochilus* + *T. sp. nov.*), (*T. tarara* + *T. lagunablanca*), (*T. teyumirim* + *T. guarani* + *T. spinulosus*), in addition to *T. melanopleurus* and *T. callathelys* as external lineages to the clade comprising all those species. mt: Strong disagreement between mitochondrial and nuclear-based phylogenies.
ASTRAL	MSA-nuc (100, 95 and 75% UCE matrices)	Species-level phylogenies	Does the species tree agree with the relationships inferred in the individual-level phylogenies?	Overall, it agrees with the IQ-TREE nuclear phylogenies.
BPP	MSA-nuc (100% matrix)	Species tree		
RelTime-Branch Lengths	Nuclear phylogenetic tree (100% UCE complete matrix)	Divergence times	When did the diversification of the *T. spinulosus* group occur? Could this temporal pattern be linked to the species' demographic history, or might it help explain gene flow events throughout their evolution?	Major divergence events occurring from 20 Ma onward. The initial split occurred between 20 and 15 Ma, with *T. melanopleurus* diverging first. Around 10 Ma, *T. callathelys* separated from the remaining taxa, while most subsequent speciation events took place between 7.5 and 2.5 Ma.
MCMCTree	MSA-nuc (100 most clocklike UCE loci selected through SortaDate)			
PhyloNetworks (SNaQ)	Unrooted nuclear gene trees (100% UCE complete matrix) + concordance factors	Phylogenetic Network	Can we detect introgression in the nuclear genome? Is evolutionary history better explained by networks or bifurcating trees in this case?	All phylogenetic network results suggest minimal or no introgression within the *T. spinulosus* species group.
PhyloNet	Rooted nuclear gene trees (100% UCE complete matrix)			
NetRAX	Unrooted nuclear gene trees (100% UCE complete matrix)			
POPART (TCS haplotype network)	Three mtDNA coding genes (COX1, COX2, and COX3)	Population structure	How is mtDNA structured in the group's lineages?	The clusters align with the groupings in the mt-phylogenetic tree, exhibiting the same pattern of discordance with the nuclear data.
D-suite (ABBA-BABA tests)	SNP	Gene flow	Is gene flow occurring between species within the *Tropidurus spinulosus* group?	Minimal interspecific nuclear admixture, suggesting that introgressive hybridization has had limited impact on the nuclear genomes of these species.
BPP (MSC-M model)	MSA-nuc (100 most clocklike UCE loci selected through SortaDate) + MSA-mt (coding + non-coding regions)	Multiple parameter estimation (mainly ancestral population sizes	Assess how gene flow differentially impacted nuclear and mitochondrial genomes	Which phylogenetic reconstruction more accurately reflects the true history of population divergence: the nuclear species tree or the mitochondrial genealogy? In

		and migration rates)		other words, is the mitochondrial genealogy a reliable representation of species history, with the nuclear tree being discordant due to factors such as incomplete lineage sorting or other processes? Or, conversely, does the nuclear tree capture the actual species relationships, while the mitochondrial genealogy is discordant due to processes like introgression or historical gene flow?
HYPHY	MSA-mt (coding regions)	Selection tests	Is there evidence of positive selection in the mitogenomes of *Tropidurus spinulosus* lineages, supporting an adaptive-based process leading to mitonuclear discordance?	Overall, there is no strong evidence of adaptive processes influencing mtDNA, with positive selection detected at only a few sites in the mitogenome.
Skyline Plot (BEAST)	MSA-mt (three partitions, comprehending six genes)	Demography tests	Estimate changes in effective population sizes over time	Demographic expansions in all analyzed species, particularly from 70 kya onward.
Stairway Plot	SNP			

Acknowledgments

We thank all the institutions that provided technical, material, and structural support during the sampling phase of this study, namely the Herpetological Collection of the University of Brasília (CHUNB), the Amphibians and Reptiles Collection of the National Institute of Amazonian Research (INPA-H), the Biosciences Institute of the University of São Paulo (IB-USP), the American Museum of Natural History (AMNH), the Museo Nacional de Historia Natural del Paraguay (MNHNP), the Mato Grosso Federal University (UFMT), Museo de Historia Natural Alcide d'Orbigny, and the Universidade Nacional de Salta (UNSa). We extend our gratitude to our esteemed colleagues Eliana Lizarraga, Felipe F. Curcio (UFMT), Karina Atkinson and Jean-Paul Brouard (Fundación Para La Tierra, Paraguay), Johanna López, Nestor Romero (and family) (Estancia Cerrados del Tagatiya), Pastor Enmanuel Pérez-Estigarribia (and family), Ricardo Céspedes, Rodrigo Ayala, and Rolando Rivas for crucial assistance or support during fieldwork. We thank Angela Coda for allowing access to the Reserva Natural Cerrados

del Tagatiya and Malvina Duarte for allowing access to the Reserva Natural Laguna Blanca. We also thank Junior Nadaline and Carlos Daniel Rivadeneira for their invaluable assistance with genetic sample processing and DNA sequencing. MTR also thanks all members of his lab for help in the field. Finally, we extend our gratitude to Prof. Renato Pires Machado (UFPR) for his valuable contributions throughout the corresponding author's PhD project.

Author contributions

Matheus Salles: study design, analyses, lead writing. Fabricius Domingos and André Carvalho: study design, field sampling, genome sequencing, writing final draft. Nicolas Martinez, Frederick Bauer, Martha Motte, Viviana Espínola, Miguel T. Rodrigues, Carla Piantoni, Guarino R. Colli, Fernanda P. Werneck: field sampling efforts and/or provision of collection materials and infrastructure. Márcio Pie, André Olivotto, Erik Choueri, Adam Leache: lab work, genome sequencing. All authors read, commented and approved the final draft of the manuscript.

Funding

This work was funded by the Brazilian National Council for Scientific and Technological Development [CNPq #200798/2010-3], the São Paulo Research Foundation [FAPESP #2011/50146-6, #2016/08249-6, #2017/20235-3, #2011/50146-6], the U.S. National Science Foundation [NSF grant #1855845], the Explorers Club, the Andrew Sabin Family Foundation, the American Museum of Natural History (Richard Gilder Graduate School), and the Brazilian funding agency ‘Coordenação de Aperfeiçoamento de Pessoal de Nível Superior’ (CAPES), which provided a PhD scholarship to the correspondent author. FPW thanks CNPq for a productivity fellowship [#307695/2023-9].

931 **Data availability**

932 The data underlying this article, including phylogenetic datasets, corresponding trees, input
933 and output files for all analyses, and any other relevant supplementary files are available in
934 Zenodo, at https://doi.org/10.5281/zenodo.15284000.

935

936 **References**

937 Allio R, et al. 2020. MitoFinder: Efficient automated large-scale extraction of mitogenomic
938 data in target enrichment phylogenomics. Molecular ecology resources 20: 892-905.

939 Andersen MJ, et al. 2021. Complex histories of gene flow and a mitochondrial capture event
940 in a non-sister pair of birds. Molecular Ecology 30: 2087–2103.
941 https://doi.org/10.1111/mec.15856

942 Andrews S. 2010. FastQC: A Quality Control Tool for High Throughput Sequence Data
943 [Online]. Available online at: http://www.bioinformatics.babraham.ac.uk/projects/fastqc/

944 Bankevich A, et al. 2012. SPAdes: a new genome assembly algorithm and its applications to
945 single-cell sequencing. Journal of computational biology 19: 455-477.

946 Benavides E, Baum R, McClellan D, Sites Jr. JW. 2007. Molecular phylogenetics of the lizard
947 genus *Microlophus* (Squamata: Tropiduridae): aligning and retrieving indel signals from
948 nuclear introns. Systematic Biology 56: 776–797.

949 Benavides E, Baum R, Snell HM, Snell HL, Sites Jr JW. 2009. Island biogeography of Galápagos
950 lava lizards (Tropiduridae: *Microlophus*): species diversity and colonization of the
951 archipelago. Evolution 63: 1606–1626.

952 Bergeron LA, et al. 2023. Evolution of the germline mutation rate across vertebrates. Nature
953 615: 285-291.

954 Bezerra CH, et al. 2025. Biogeographical Origins of Caatinga Squamata Fauna. Journal of
955 Biogeography 52: 521-531.

956 Bolger AM, Lohse M, Usadel B. 2014. Trimmomatic: a flexible trimmer for Illumina sequence
957 data. Bioinformatics 30: 2114-2120.

958 Bonnet T, Leblois R, Rousset F, Crochet PA. 2017. A reassessment of explanations for
959 discordant introgressions of mitochondrial and nuclear genomes. Evolution 71: 2140-2158.

Borowiec ML. 2016. AMAS: a fast tool for alignment manipulation and computing of summary statistics. PeerJ 4: e1660.

Bouckaert R, et al. 2019. BEAST 2.5: An advanced software platform for Bayesian evolutionary analysis. PLoS computational biology 15: e1006650.

Burbrink FT, Gehara M, McKelvy AD, Myers EA. 2021. Resolving spatial complexities of hybridization in the context of the gray zone of speciation in North American ratsnakes (*Pantherophis obsoletus* complex). Evolution 75: 260-277.

Bushnell B. 2018. BBTools: a suite of fast, multithreaded bioinformatics tools designed for analysis of DNA and RNA sequence data. *Joint Genome Institute*.

Cai R, Ané C. 2021. Assessing the fit of the multi-species network coalescent to multi-locus data. Bioinformatics 37: 634-641.

Camurugi F, et al. 2022. Isolation by distance and past climate resistance shaped the distribution of genealogical lineages of a neotropical lizard. Systematics and Biodiversity 20: 1-19.

Carvalho ALG. 2013. On the distribution and conservation of the South American lizard genus *Tropidurus* Wied-Neuwied, 1825 (Squamata: Tropiduridae). Zootaxa 3640: 42–56.

2016. Three New Species of the *Tropidurus spinulosus* Group (Squamata: Tropiduridae) from Eastern Paraguay. American Museum Novitates 3853: 1–44, doi:10.1206/3853.1

Carvalho ALG, de Britto MR, Fernandes DS. 2013. Biogeography of the Lizard Genus *Tropidurus* Wied-Neuwied, 1825 (Squamata: Tropiduridae): Distribution, Endemism, and Area Relationships in South America. PLoS One: 8.

Carvalho ALG, et al. 2016. A New *Tropidurus* (Tropiduridae) from the Semiarid Brazilian Caatinga: Evidence for Conflicting Signal between Mitochondrial and Nuclear Loci Affecting the Phylogenetic Reconstruction of South American Collared Lizards. American Museum Novitates 3852: 1–68.

Carvalho ALG, et al. 2024. A highly polymorphic South American collared lizard (Tropiduridae: *Tropidurus*) reveals that open–dry refugia from South-western Amazonia staged allopatric speciation. Zoological Journal of the Linnean Society 201: 493-533.

Castresana J. 2000. Selection of conserved blocks from multiple alignments for their use in phylogenetic analysis. Molecular biology and evolution 17: 540-552.

Chung DJ, Schulte PM. 2020. Mitochondria and the thermal limits of ectotherms. Journal of Experimental Biology 223: jeb227801.

Clement M, Snell Q, Walke P, Posada D, Crandall K. 2002. TCS: estimating gene genealogies. In *Parallel and distributed processing symposium, international* (Vol. 2, pp. 7-pp). IEEE Computer Society.

DeRaad DA. 2022. SNPfiltR: an R package for interactive and reproducible SNP filtering. Molecular Ecology Resources 22: 2443-2453.

DeRaad DA, et al. 2023. Mitonuclear discordance results from incomplete lineage sorting, with no detectable evidence for gene flow, in a rapid radiation of *Todiramphus* kingfishers. Molecular Ecology 32: 4844–4862. https://doi.org/10.1111/mec.17080

Després L. 2019. One, two or more species? Mitonuclear discordance and species delimitation. Molecular Ecology 28: 3845–3847. https://doi.org/10.1111/mec.15211

Dessi MC, et al. 2022. The role of sex-biased dispersion in promoting mitonuclear discordance in *Partamona helleri* (Hymenoptera: Apidae: Meliponini). Biological Journal of the Linnean Society 136: 423-435.

Dong X, et al. 2023. Mitochondrial introgression and mito-nuclear discordance obscured the closely related species boundaries in Cletus Stål from China (Heteroptera: Coreidae). Molecular Phylogenetics and Evolution 184. https://doi.org/10.1016/j.ympev.2023.107802

Dufresnes C, et al. 2020. Are glacial refugia hotspots of speciation and cytonuclear discordances? Answers from the genomic phylogeography of Spanish common frogs. Molecular Ecology 29: 986–1000. https://doi.org/10.1111/mec.15368

Durand EY, Patterson N, Reich D, Slatkin M. 2011. Testing for ancient admixture between closely related populations. Molecular Biology and Evolution 28: 2239-2252.

Excoffier L, Foll M, Petit RJ. 2009. Genetic consequences of range expansions. Annual Review of Ecology, Evolution, and Systematics 40: 481-501.

Faircloth BC, et al. 2012. Ultraconserved elements anchor thousands of genetic markers spanning multiple evolutionary timescales. Systematic Biology 61: 717-26.

Faircloth BC. 2016. PHYLUCE is a software package for the analysis of conserved genomic loci. Bioinformatics 32: 786–788.

Fedorov VB, Trucchi E, Goropashnaya AV, Stenseth NC. 2022. Conflicting nuclear and mitogenome phylogenies reveal ancient mitochondrial replacement between two North American species of collared lemmings (*Dicrostonyx groenlandicus*, *D. hudsonius*). Molecular phylogenetics and evolution 168.

1024 Firneno TJ, et al. 2021. Delimitation despite discordance: Evaluating the species limits of a
1025 confounding species complex in the face of mitonuclear discordance. Ecology and Evolution
1026 11: 12739–12753. https://doi.org/10.1002/ece3.8018

1027 Flouri T, Jiao X, Rannala B, Yang Z. 2018. Species Tree Inference with BPP using Genomic
1028 Sequences and the Multispecies Coalescent. Molecular Biology and Evolution 35: 2585-2593.
1029 doi:10.1093/molbev/msy147

1030 Flouri T, Jiao X, Huang J, Rannala B, Yang Z. 2023. Efficient Bayesian inference under the
1031 multispecies coalescent with migration. Proceedings of the National Academy of
1032 Sciences 120: e2310708120.

1033 Frost DR, Crafts HM, Fitzgerald LA, Titus TA. 1998. Geographic variation, species recognition,
1034 and molecular evolution of cytochrome oxidase I in the *Tropidurus spinulosus* complex
1035 (Iguania: Tropiduridae). Copeia: 839-851.

1036 Good JM, Vanderpool D, Keeble S, Bi K. 2015. Negligible nuclear introgression despite
1037 complete mitochondrial capture between two species of chipmunks. Evolution 69: 1961–
1038 1972. https://doi.org/10.1111/evo.12712

1039 Guillory WX, Brown JL. 2021. A new method for integrating ecological niche modeling with
1040 phylogenetics to estimate ancestral distributions. Systematic Biology 70: 1033-1045.

1041 Guillory WX, et al. 2024. Geoclimatic drivers of diversification in the largest arid and semi-
1042 arid environment of the Neotropics: Perspectives from phylogeography. Molecular Ecology
1043 e17431.

1044 Gutenkunst RN, Hernandez RD, Williamson SH, Bustamante CD. 2009. Inferring the joint
1045 demographic history of multiple populations from multidimensional SNP data. PLoS
1046 Genetics, 5:e1000695

1047 Harris RS. 2007. *Improved pairwise alignment of genomic DNA*. The Pennsylvania State
1048 University.

1049 Harvey MB, Gutberlet Jr RL. 1998. Lizards of the genus *Tropidurus* (Iguania: Tropiduridae)
1050 from the Serranía de Huanchaca, Bolivia: new species, natural history, and a key to the
1051 genus. Herpetologica 493-520.

1052 Harvey MG, Smith BT, Glenn TC, Faircloth BC, Brumfield RT. 2016. Sequence capture versus
1053 restriction site associated DNA sequencing for shallow systematics. Systematic Biology 65:
1054 910-924.

1055 Heled J, Drummond AJ. 2008. Bayesian inference of population size history from multiple
1056 loci. BMC evolutionary biology 8: 1-15.

1057 Hibbins MS, Hahn MW. 2022. Phylogenomic approaches to detecting and characterizing
1058 introgression. Genetics 220.

1059 Hinojosa JC, et al. 2019. A mirage of cryptic species: Genomics uncover striking mitonuclear
1060 discordance in the butterfly *Thymelicus sylvestris*. Molecular Ecology 28: 3857–3868.
1061 https://doi.org/10.1111/mec.15153

1062 Kalyaanamoorthy S, Minh BQ, Wong TK, Von Haeseler A, Jermiin LS. 2017. ModelFinder: fast
1063 model selection for accurate phylogenetic estimates. Nature methods 14: 587-589.

1064 Katoh K, Standley DM. 2013. MAFFT multiple sequence alignment software version 7:
1065 improvements in performance and usability. Molecular biology and evolution 30: 772-780.

1066 Knaus BJ, Grünwald NJ. 2017. vcfr: a package to manipulate and visualize variant call format
1067 data in R. Molecular Ecology Resources 17: 44-53.

1068 Leigh JW, Bryant D, Nakagawa S. 2015. POPART: full-feature software for haplotype network
1069 construction. Methods in Ecology & Evolution 6.

1070 Li H, et al. 2009. The sequence alignment/map format and SAMtools. Bioinformatics 25:
1071 2078-2079.

1072 Li H. 2013. Aligning sequence reads, clone sequences and assembly contigs with BWA-MEM.
1073 arXiv:1303.3997v2 [q-bio.GN].

1074 Liu X, Fu YX. 2020. Stairway Plot 2: demographic history inference with folded SNP frequency
1075 spectra. Genome biology 21: 280.

1076 Lutteropp S, Scornavacca C, Kozlov AM, Morel B, Stamatakis A. 2022. NetRAX: accurate and
1077 fast maximum likelihood phylogenetic network inference. Bioinformatics 38: 3725-3733.

1078 Malinsky M, Matschiner M, Svardal H. 2021. Dsuite-Fast D-statistics and related admixture
1079 evidence from VCF files. Molecular ecology resources 21: 584-595.

1080 Mao X, Rossiter SJ. 2020. Genome-wide data reveal discordant mitonuclear introgression in
1081 the intermediate horseshoe bat (*Rhinolophus affinis*). Molecular phylogenetics and
1082 evolution, 150: 106886.

1083 McKenna A, et al. 2010. The Genome Analysis Toolkit: a MapReduce framework for analyzing
1084 next-generation DNA sequencing data. Genome research 20: 1297-1303.

1085 Minh BQ, et al. 2020. IQ-TREE 2: new models and efficient methods for phylogenetic
1086 inference in the genomic era. Molecular biology and evolution 37: 1530-1534.

Moore WS. 1995. Inferring phylogenies from mtDNA variation: mitochondrial-gene trees versus nuclear-gene trees. Evolution 49: 718-726.

Murrell B, et al. 2012. Detecting individual sites subject to episodic diversifying selection. PLoS genetics 8: e1002764.

Murrell B, et al. 2013. FUBAR: a fast, unconstrained bayesian approximation for inferring selection. Molecular biology and evolution 30: 1196-1205.

Murrell B, et al. 2015. Gene-wide identification of episodic selection. Molecular biology and evolution 32: 1365-1371.

Myers EA, et al. 2022. Interspecific gene flow and mitochondrial genome capture during the radiation of Jamaican *Anolis* lizards (Squamata: Iguanidae). Systematic Biology 71: 501-511.

Olson DM, et al. 2001. Terrestrial ecoregions of the world: a new map of life on Earth. BioScience 51: 933–938.

Palacios C, Campagna L, Parra JL,Cadena CD. 2023. Mito-nuclear discordance in the phenotypically variable Andean hummingbirds *Coeligena bonapartei* and *Coeligena helianthea* (Trochilidae). Biological Journal of the Linnean Society 139: 145-157.

Paradis E. 2010. pegas: an R package for population genetics with an integrated–modular approach. Bioinformatics 26: 419-420.

Phuong MA, Bi K, Moritz C. 2016. Range instability leads to cytonuclear discordance in a morphologically cryptic ground squirrel species complex. Molecular Ecology 26: 4743–4755. https://doi.org/10.1111/mec.14238

Purcell S, et al. 2007. PLINK: a tool set for whole-genome association and population-based linkage analyses. The American journal of human genetics 81: 559-575.

Qi Y, Yang W, Lu B, Fu J. 2013. Genetic evidence for male-biased dispersal in the Qinghai toad-headed agamid *Phrynocephalus vlangalii* and its potential link to individual social interactions. Ecology & Evolution 3: 1219-1230.

Rambaut A, Drummond AJ. 2014. LogCombiner v2. 1.3. Edinburgh (UK): Institute of Evolutionary Biology, University of Edinburgh.

Rambaut A. 2014. FigTree v.1.4.2: tree drawing tool. Available at: http://tree.bio.ed.ac.uk/software/figtree/

Rambaut A, Drummond AJ, Xi D, Baele G, Suchard MA. 2018. Posterior summarization in Bayesian phylogenetics using Tracer 1.7. Systematic biology 67: 901-904.

1118 Rancilhac L, et al. 2021. Phylotranscriptomic evidence for pervasive ancient hybridization
1119 among Old World salamanders. Molecular Phylogenetics and Evolution, 155.
1120 https://doi.org/10.1016/j.ympev.2020.106967

1121 Raposo do Amaral F, et al. 2018. Recent chapters of Neotropical history overlooked in
1122 phylogeography: Shallow divergence explains phenotype and genotype uncoupling in
1123 *Antilophia* manakins. Molecular ecology 27: 4108-4120.

1124 dos Reis M, Yang Z. 2019. Bayesian molecular clock dating using genome-scale datasets.
1125 *Evolutionary genomics: Statistical and computational methods*, 309-330.

1126 Roux C, et al. 2016. Shedding light on the grey zone of speciation along a continuum of
1127 genomic divergence. PLoS biology 14.

1128 Seixas FA, Boursot P, Melo-Ferreira J. 2018. The genomic impact of historical hybridization
1129 with massive mitochondrial DNA introgression. Genome Biology 19.
1130 https://doi.org/10.1186/s13059-018-1471-8

1131 Shen CC, Miura I, Lin TH, Toda M, Nguyen HN, Tseng HY, & Lin SM. 2025. Exploring
1132 Mitonuclear Discordance: Ghost Introgression From an Ancient Extinction Lineage in the
1133 *Odorrana swinhoana* Complex. Molecular Ecology e17763.

1134 Smith BT, Harvey MG, Faircloth BC, Glenn TC, Brumfield RT. 2014. Target Capture and
1135 Massively Parallel Sequencing of Ultraconserved Elements (UCEs) for Comparative Studies at
1136 Shallow Evolutionary Time Scales. Syst Biol 64: 83-95. doi:10.1093/sysbio/syt061.

1137 Smith MD, et al. 2015. Less is more: an adaptive branch-site random effects model for
1138 efficient detection of episodic diversifying selection. Molecular biology and evolution 32:
1139 1342-1353.

1140 Smith SA, Brown JW, Walker JF. 2018. So many genes, so little time: a practical approach to
1141 divergence-time estimation in the genomic era. PloS one 13: e0197433.

1142 Solís-Lemus C, Ané C. 2016. Inferring phylogenetic networks with maximum
1143 pseudolikelihood under incomplete lineage sorting. PLoS genetics 12: e1005896.

1144 Solís-Lemus C, Yang M, Ané C. 2016. Inconsistency of species tree methods under gene flow.
1145 Systematic biology 65: 843-851.

1146 Solís-Lemus C, Bastide P, Ané C. 2017. PhyloNetworks: a package for phylogenetic networks.
1147 Molecular biology and evolution 34: 3292-3298.

1148 Stankowski S, Ravinet M. 2021. Defining the speciation continuum. Evolution 75: 1256-1273.

Tamura K, Qiqing T, Kumar S. 2018. Theoretical Foundation of the RelTime Method for Estimating Divergence Times from Variable Evolutionary Rates. Molecular Biology and Evolution 35: 1770-1782.

Tamura K, Stecher G, Kumar S. 2021. MEGA 11: Molecular Evolutionary Genetics Analysis Version 11. Molecular Biology and Evolution. https://doi.org/10.1093/molbev/msab120.

Tao Q, Tamura K. Mello B, Kumar S. 2020. Reliable Confidence Intervals for RelTime Estimates of Evolutionary Divergence Times. Molecular Biology and Evolution 37: 280-290.

Toews DP, Brelsford A. 2012. The biogeography of mitochondrial and nuclear discordance in animals. Molecular ecology 21: 3907-3930.

Wen D, Yu Y, Zhu J, Nakhleh L. 2018. Inferring phylogenetic networks using PhyloNet. Systematic biology 67: 735-740.

Werneck FP, Leite RN, Geurgas SR, Rodrigues MT. 2015. Biogeographic history and cryptic diversity of saxicolous Tropiduridae lizards endemic to the semiarid Caatinga. BMC Evolutionary Biology 15: 1-24.

Zarza E, et al. 2016. Hidden histories of gene flow in highland birds revealed with genomic markers. Molecular Ecology, 25: 5144-5157.

Zhang C, Rabiee M, Sayyari E, Mirarab S. 2018. ASTRAL-III: polynomial time species tree reconstruction from partially resolved gene trees. BMC bioinformatics 19: 15-30.

Zheng Y, Wiens JJ. 2016. Combining phylogenomic and supermatrix approaches, and a time-calibrated phylogeny for squamate reptiles (lizards and snakes) based on 52 genes and 4162 species. Molecular phylogenetics and evolution 94: 537-547.

Zieliński P, et al. 2013. No evidence for nuclear introgression despite complete mtDNA replacement in the Carpathian newt (*Lissotriton montandoni*). Molecular Ecology 22: 1884-1903.